SCIENCE AND TECHNOLOGY ORGANIZATION
CENTRE FOR MARITIME RESEARCH AND EXPERIMENTATION

Reprint Series

CMRE-PR-2014-014

Maritime surveillance using multiple high-frequency surface-wave radars

Salvatore Maresca, Paolo Braca, Jochen Horstmann, Raffaele Grasso

May 2014

Originally published in:

IEEE Transactions on Geoscience and Remote Sensing, Vol. 52 (8), 2014, pp. 5056-5071.

About CMRE

The Centre for Maritime Research and Experimentation (CMRE) is a world-class NATO scientific research and experimentation facility located in La Spezia, Italy.

The CMRE was established by the North Atlantic Council on 1 July 2012 as part of the NATO Science & Technology Organization. The CMRE and its predecessors have served NATO for over 50 years as the SACLANT Anti-Submarine Warfare Centre, SACLANT Undersea Research Centre, NATO Undersea Research Centre (NURC) and now as part of the Science & Technology Organization.

CMRE conducts state-of-the-art scientific research and experimentation ranging from concept development to prototype demonstration in an operational environment and has produced leaders in ocean science, modelling and simulation, acoustics and other disciplines, as well as producing critical results and understanding that have been built into the operational concepts of NATO and the nations.

CMRE conducts hands-on scientific and engineering research for the direct benefit of its NATO Customers. It operates two research vessels that enable science and technology solutions to be explored and exploited at sea. The largest of these vessels, the NRV Alliance, is a global class vessel that is acoustically extremely quiet.

CMRE is a leading example of enabling nations to work more effectively and efficiently together by prioritizing national needs, focusing on research and technology challenges, both in and out of the maritime environment, through the collective Power of its world-class scientists, engineers, and specialized laboratories in collaboration with the many partners in and out of the scientific domain.

NOTE: The CMRE Reprint series reprints papers and articles published by CMRE authors in the open literature as an effort to widely disseminate CMRE products. Users are encouraged to cite the original article where possible.

Maritime Surveillance Using Multiple High-Frequency Surface-Wave Radars

Salvatore Maresca, Paolo Braca, Jochen Horstmann, and Raffaele Grasso

***Abstract*—In the last decades, great interest has been directed toward low-power high-frequency (HF) surface-wave radars as long-range early warning tools in maritime-situational-awareness applications. These sensors, developed for ocean remote sensing, provide an additional source of information for ship detection and tracking, by virtue of their over-the-horizon coverage capability and continuous-time mode of operation. Unfortunately, they exhibit many shortcomings that need to be taken into account, such as poor range and azimuth resolution, high nonlinearity, and significant presence of clutter. In this paper, radar detection, multitarget tracking, and data fusion (DF) techniques are applied to experimental data collected during an HF-radar experiment, which took place between May and December 2009 on the Ligurian coast of the Mediterranean Sea. The system performance is defined in terms of time on target (ToT), false alarm rate (FAR), track fragmentation, and accuracy. A full statistical characterization is provided using one month of data. The effectiveness of the tracking and DF procedures is shown in comparison to the radar detection algorithm. In particular, the detector's FAR is reduced by one order of magnitude. Improvements, using the DF of the two radars, are also reported in terms of ToT as well as accuracy.**

***Index Terms*—Data fusion (DF), high-frequency (HF) surface wave (HFSW) radar, maritime surveillance, sea clutter, target detection, target tracking.**

I. Introduction

MARITIME surveillance represents a primary concern for both national and international communities. The broad range of requirements is intended for supporting the protection and the exercise of national sovereignty, not only in terms of law enforcement but also in terms of search and rescue, environmental protection, and resource management. In maritime-situational-awareness activities, sensor integration is vital for granting clear pictures of the surveyed areas. On the other hand, this domain continuously brings on new challenges related to the nature of the sensors, their characteristics, and the type of information that they provide.

The traditional monitoring systems suffer from physical limitations. For instance, standard microwave radars operate only within line-of-sight propagation, with a maximum range of some dozens of kilometers, while satellite sensors (e.g., synthetic aperture radars) cannot grant a continuous temporal coverage of the region of interest with an adequate level of real-time surveillance. High-frequency (HF) surface wave (HFSW) radar systems can fulfill many of these limitations and provide additional information on the vessel traffic, by virtue of their capability of detecting targets over-the-horizon, their continuous-time coverage, and their direct target velocity estimation through the Doppler data [1]. An important characteristic of these systems is that very low power is required to operate a single radar site, about 35 W on average.

HFSW radars work in the 3–30 MHz band, with wavelengths between 100 and 10 m, respectively. In this interval, vertically polarized radio waves have also the ability to propagate as surface waves [2], [3]. Low-power HFSW radar systems have been developed mainly for ocean remote sensing applications, e.g., surface currents and sea-state mapping, wind extraction, wave spectra analysis, and, recently, tsunami early warning detection [4]. There are many commercial systems, e.g., the Coastal Ocean Dynamics Applications Radar (CODAR), developed at the National Oceanic and Atmospheric Administration (NOAA) [5], and the Wellen radar (WERA), developed at the University of Hamburg [6]. These systems can be found mainly operating from the coast, while only a few experiments have been conducted with shipborne installations.

The idea is to take advantage of the growing number of oceanographic HFSW radars along the coasts also for maritime-surveillance applications. Hence, ship detection and sea-state sensing become two complementary problems. In fact, the presence of clutter is unwelcome as far as we are interested in ship detection, while the presence of ships can limit the extraction of oceanographic parameters [7]. For this reason, in the past years, much interest has been focused to develop new spectral models for modeling the return from the sea, with the ultimate goals of enhancing both the target detection via clutter-suppression techniques [8] and the ocean sensing [9], [10]. Since the system is set up for oceanic parameter estimation, its configuration is not optimal for target detection. This represents a further problem since the signal environment already includes external noise, different types of clutter, and interference, which can significantly degrade the detection performance. Poor range and azimuth resolution compared to microwave radars, high nonlinearity in the state/measurement space, significant false alarm rate (FAR) due to both sea clutter and man-made/natural interference, and the crowding of the HF spectrum [6] are all problems to cope with. It is worth noting that the underlying physics which regulate the signal transmission and backscattering in

Manuscript received June 25, 2013; revised August 29, 2013; accepted October 13, 2013. This work was supported by the NATO Allied Command Transformation (NATO-ACT) under the project ACT000215, Maritime Situational Awareness (MSA).

S. Maresca, P. Braca, and R. Grasso are with North Atlantic Treaty Organization (NATO) Science and Technology Organization (STO) Centre for Maritime Research and Experimentation, 19126 La Spezia, Italy (e-mail: maresca@cmre.nato.int; braca@cmre.nato.int; grasso@cmre.nato.int).

J. Horstmann is with Helmholtz-Zentrum Geesthacht, 21502 Geesthacht, Germany, and also with NATO STO Centre for Maritime Research and Experimentation, 19126 La Spezia, Italy (e-mail: jochen.horstmann@hzg.de).

Color versions of one or more of the figures in this paper are available online at http://ieeexplore.ieee.org.

Digital Object Identifier 10.1109/TGRS.2013.2286741

the HF band are quite different from that of the common microwave region. An overview of the main theoretical elements for modeling the backscatter signal can be found in [1], while in [11] and [12], a simulator has been proposed for generating the signal received by an HF system and for performing detection and tracking of targets. The analysis and modeling of sea clutter and noise sources both in the amplitude and frequency domains have been presented and discussed in [13] and [14].

Modern multitarget tracking (MTT) and data fusion (DF) techniques are mandatory in order to deal with the aforementioned shortcomings and to obtain operationally acceptable performance. In the last few years, great progress has been made, both at theoretical and practical levels, and many approaches and paradigms have emerged in the MTT and DF literature [15], [16]. Among these, we mention the multiple hypothesis tracking (MHT) [15], [17], the joint probabilistic data association (JPDA) rule [15], [18], the sequential Monte Carlo methods [19], [20], and the probability hypothesis density (PHD) filter [16], [21]–[24].

While the MTT strategies are normally applied to many scientific fields, e.g., antisubmarine warfare [25], video surveillance [26], and coastal monitoring [18], less is known about their performance bounds and their fundamental limits. In [22] and [23], the authors have proven that the multisensor PHD function behaves, by increasing the number of sensors, as a mixture of as many Gaussian components as the true number of targets. These Gaussian functions become progressively narrower and peakier around the true target states in a way that is ruled by the Fisher information [22]. In other words, the multisensor PHD is asymptotically optimal. However, the main drawback of this methodology is that a computationally efficient algorithm still needs to be developed. The work presented in [24] goes in this direction.

A quantitative comparison among the MTT strategies is provided in [27], where the techniques have been categorized into more than 35 different algorithmic typologies. The comparison is provided in such a way that lists each algorithm and categorizes the processing scheme, data association mechanism, complexity scaling (with the number of targets and with the state dimension), overall complexity, and a subjective performance figure.

This paper provides a first attempt to fully characterize the detection, tracking, and DF performance of a suitable MTT-DF strategy applied to the data recorded by two WERA systems. The experimentation has been conducted by the NATO Science and Technology Organization Centre for Maritime Research and Experimentation during the Battlespace Preparation 2009 (BP09) HF-radar campaign in the Ligurian Sea (Mediterranean Sea).

Radar detection is performed using a 3-D (range-azimuth-Doppler) ordered statistics (OS) constant false alarm rate (CFAR) algorithm [28]. As it will be presented in the following, the detection procedure exhibits a high number of clutter returns, due to both sea clutter and interference. This problem is addressed by exploiting the JPDA rule. It is worth noting that the JPDA has lower performance than the MHT and the PHD but, interestingly, requires also a lower complexity, comparable with the Kalman filter that is the simplest possible solution. In fact, a common feature of the MHT algorithm is the exponentially increasing number of hypotheses, which necessitates pruning procedures, while the PHD requires techniques such as particle filtering (PF) that are computationally demanding [27].

Another problem arises from the strong nonlinearity present in the use of the Doppler measurements. Two possible solutions are commonly used in MTT problems: tracking in mixed coordinates and tracking in Cartesian coordinates. The former approach is based on the extended Kalman filter (EKF), which can suffer from high nonlinearity and lead to a rapid divergence of the filter itself. In the second approach, measurements in sensor coordinates are converted to Cartesian coordinates. The converted measurement error covariance can be quite large for far-range targets, which is the case of HFSW radars. The unscented Kalman filter (UKF) addresses the flaws of the EKF by using a deterministic sampling approach [29], which is computationally much less onerous than a PF. The state distribution is a Gaussian random vector, whose posterior mean and covariance are accurately estimated using a minimal set of carefully chosen sigma points [29]. In order to cope with strong clutter and nonlinearity, the JPDA-UKF algorithm has been successfully applied to HFSW radars, as already presented in [30].

A proper DF technique applied to multiple radar sensors can provide a sensible gain in terms of performance. In this paper, two simultaneously operating HFSW radars with overlapping fields of view are considered. A hierarchical DF strategy is successfully adopted in which the tracks generated by the MTT at each site are combined by a track-to-track association and fusion (T2T-A/F) logic (see details in [15]). Preliminary results on the DF applied to HFSW radars have been presented in [31].

A set of *ad hoc* performance metrics is defined to compare the signal processing chain from the detection to the fusion: 1) the pair ToT and FAR; 2) track fragmentation (TF); and 3) root-mean-square error (RMSE) of the target position and velocity. The ToT is the percent of time that a target is successfully observed by the system, while the FAR is the normalized number of false tracks (or detections) generated in the surveillance region per unit of space and time. The TF is quantitatively characterized by the ToT and the number of subtracks associated with the same target. Ideally, we would like to have 100% as ToT with just a single track, while a bad system would generate a low ToT with several tracks. The RMSE is a measure of the accuracy of the radar system. Tracks and detections are validated or labeled as false using ship reports from the Automatic Identification System (AIS), used as ground-truth information. Unfortunately, there are several vessels that are not cooperative, in the sense that they do not provide any AIS reports (e.g., fishing boats and warships). Consequently, the FAR that is computed represents a kind of worst case.

This paper is organized as follows. In Section II, the NATO BP09 experiment on HF radars is presented. The MTT-DF system is described in Section III. In Section IV, both the AIS and HF data formats, the association procedure, and the performance metrics are presented. Experimental results are shown and discussed in Section V, while conclusions and guidelines for future work are provided in Section VI.

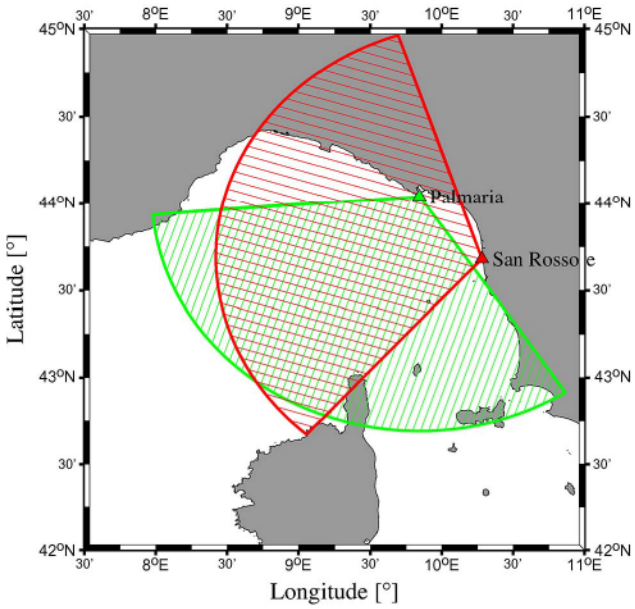

Fig. 1. Picture of the NATO BP09 experiment on HF-radars. (Green) Palmaria and (red) San Rossore sites and covered areas.

II. HF-Radar Experiment

A. Experiment Setup

Two WERA systems were deployed on the Italian coast of the Ligurian Sea, one on Palmaria island near La Spezia (44° 2′ 30″ N, 9° 50′ 36″ E) and the other at San Rossore park near Pisa (43° 40′ 53″ N, 10° 16′ 52″ E), as depicted in Fig. 1.

WERA is a quasi-monostatic system, whose transmitter (Tx) and receiver (Rx) are made up with $\lambda_0/4$ monopole arrays, where λ_0 is the carrier wavelength. The distance between Tx and Rx is approximately 300 m. In the ground-based installation setup, the transmitter has a rectangular arrangement, while during the experiment, the receiver was made by a 16-element linear array. The angles w.r.t. north of the two array installations are 296.2° and 12.0°, respectively. The azimuth information is extracted via a beamforming procedure of the received data, using the Hamming window, with a field of view of 120° around the broadside direction. WERA systems use linear frequency-modulated continuous-wave chirps. The two systems use the same operating frequency (i.e., $f_0 = 12.5$ MHz), with orthogonal modulating waveforms. The range resolution was $\Delta R = 1.5$ km, with chirp bandwidth $B = 100$ kHz. Both systems were operated at approximately 35 W on average.

Target detection is performed in the Doppler domain by a 3-D OS-CFAR algorithm, developed at the University of Hamburg [28]. Coherent processing intervals (CPIs), not statistically independent, are made of 512 (or 256) samples with an overlap of 75%, i.e., a detection occurs every 33.28 s (or 16.64 s). AIS ship reports are provided by the base station located at Castellana (44° 4′ 3″ N, 9° 48′ 58″ E, at a 200 m altitude).

B. Range-Doppler Power Spectrum

As stated in Section I, the underlying physics of signal transmission and backscattering in the HF-band are different

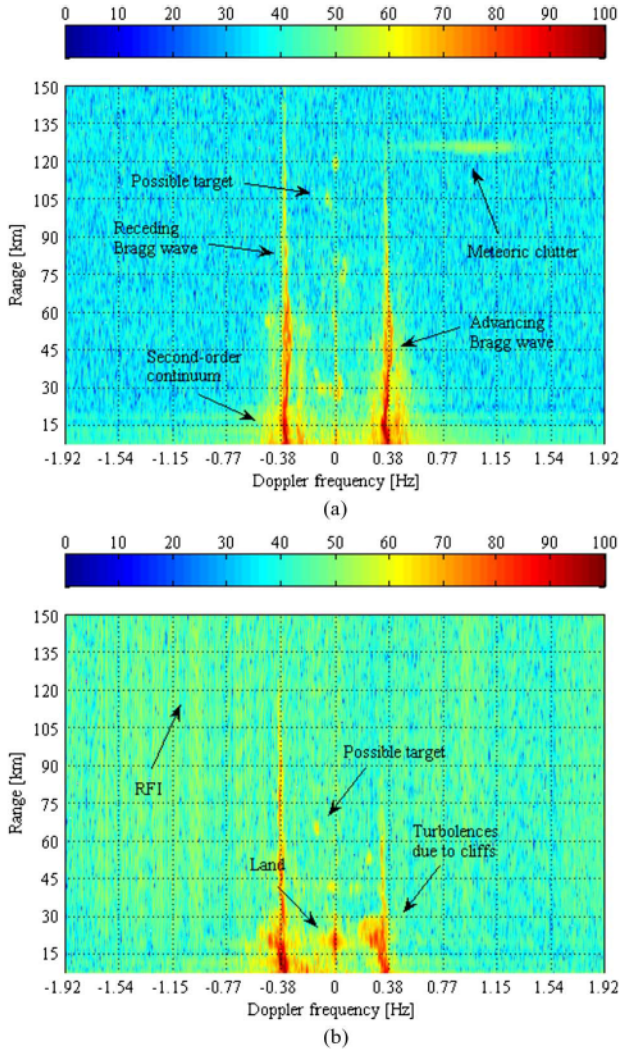

Fig. 2. Typical range-Doppler power spectra in the HF-band, retrieved from field data. Subfigure (a): Sea clutter, meteoric clutter, and possible ship returns. Subfigure (b): Sea clutter, RFI, land scattering, and possible ship returns.

from that in the S- and X-bands commonly exploited by marine radars. The contribution of sea clutter is produced by specific spectral components of the surface-height wave field, as depicted by two typical range-Doppler power spectra in Fig. 2. The main features (i.e., the two lines extending along range) are due to the first-order Bragg scattering and are generated by those gravity waves of half the radar wavelength, traveling toward and away from the radar site. The separation between the two Bragg velocities Δf is given by [32]

$$\Delta f = 2\sqrt{\frac{g f_0}{\pi c}} \tag{1}$$

where g is the acceleration due to gravity, c is the speed of light, and $f_0 = c/\lambda_0$ is the center-band frequency. During the experiment, Δf was about 0.72 Hz. However, these frequencies can deviate from the theoretical values in nonmoving waters according to underlying surface currents.

The second-order Bragg scattering generates sideband contributions in the range-Doppler spectrum and is responsible of the directional wave spectrum. With increasing distance, sea

clutter tends to become a white random process. According to where the system is installed, land-scattered echoes around the zero frequency can also be observed [see Fig. 2(b)]. In this case, sea clutter harmonics may undergo a sort of frequency modulation due to rapid changes in the sea wave movement around rock cliffs [14]. The theoretical modeling of the backscatter signal is addressed in [1].

In addition, a variety of interference sources, both natural and man-made, can degrade the reception of ship echoes. Natural interference consist of unwanted propagation modes through the ionosphere or meteor trail echoes [see Fig. 2(a)]. They manifest by means of large horizontal returns that can cover large portions of the Doppler space at far range.

Radio frequency interference (RFI) is also present and manifests as vertical lines (i.e., constant along range and at given frequencies) in the range-Doppler spectrum [see Fig. 2(b)]. Furthermore, as shown in Fig. 2, spurious peaks can be observed, mainly distributed between the two first-order Bragg frequencies. Some of these returns can be generated by targets, while some others instead repeat with a range periodicity. They are probably due to unwanted coupling effects with the 50 Hz feeding network. At last, a not perfectly zero back radiation of the transmitter can be observed at near ranges.

III. MTT and DF Procedure

In this section, the MTT-DF system is introduced, based on the state of the art in target tracking and DF literature [15]. First, we describe the target motion and measurement models of the HFSW radar, then the MTT algorithm operating at the single radar site, and, finally, the DF procedure which combines the information from each radar.

In MTT systems, the *track management* process can be broadly divided into *track initiation*, *track update*, and *track elimination*. Track update is performed by the *data association*, which determines how detections (clutter- and target-originated measurements) are associated to the existing tracks, and by the *track filtering* steps, which include the target motion model used to predict and to update the target state of the tracks.

The DF is based on the T2T paradigm, which combines the tracks at each radar site in order to obtain a set of *fused* tracks containing the whole information collected by the remote radars.

A. Target Motion and Measurement Models

The target state vector $\boldsymbol{x}_k$ at time k is defined in Cartesian coordinates

$$\boldsymbol{x}_k = ([x_k, \dot{x}_k, y_k, \dot{y}_k])^T \tag{2}$$

where x_k, y_k and $\dot{x}_k, \dot{y}_k$ are the position and velocity components along the x, y directions, respectively, and $(\cdot)^T$ is the transpose operator. In the majority of cases, the motion of large vessels can be described with the nearly constant velocity model [15]. The state-update equation is [15], [33]

$$\boldsymbol{x}_k = \boldsymbol{F}_k \boldsymbol{x}_{k-1} + \boldsymbol{\Gamma}_k \boldsymbol{v}_k. \tag{3}$$

The motion relation matrices $\boldsymbol{F}_k = \mathrm{diag}([F_k, F_k])$ and $\boldsymbol{\Gamma}_k = \mathrm{diag}([\Gamma_k, \Gamma_k])$ are

$$F_k = \begin{bmatrix} 1 & T_k \\ 0 & 1 \end{bmatrix}, \quad \Gamma_k = \begin{bmatrix} T_k^2/2 \\ T_k \end{bmatrix} \tag{4}$$

where $\mathrm{diag}(\cdot)$ is the block diagonal matrix operator, while T_k is the time interleaved between sampling times $k-1$ and k. This time corresponds to the 25% of the CPI [28] (see Section II). Vector $\boldsymbol{v}_k$ takes into account the target acceleration and the unmodeled dynamics and is assumed to be Gaussian with zero-mean and covariance matrix $\boldsymbol{Q}_k = \mathrm{diag}(\sigma_v^2, \sigma_v^2)$. Measurement vector $\boldsymbol{z}_k$ is defined as

$$\boldsymbol{z}_k \triangleq \left([z_k^r, z_k^b, z_k^{\dot{r}}]\right)^T \tag{5}$$

where z_k^r, z_k^b, and $z_k^{\dot{r}}$ are the measured range, bearing, and range rate, respectively. Let us fix the origin of axes at the radar site, approximating the quasi-monostatic setup with a monostatic setup (note that the distance between Tx and Rx is just 300 m). The target-originated measurement equation is thus

$$\boldsymbol{z}_k = \mathrm{h}(\boldsymbol{x}_k) + \boldsymbol{n}_k \tag{6}$$

where

$$\mathrm{h}(\boldsymbol{x}_k) \triangleq \left(\left[\sqrt{x_k^2 + y_k^2}, \arctan\left(\frac{y_k}{x_k}\right), \frac{x_k \dot{x}_k + y_k \dot{y}_k}{\sqrt{x_k^2 + y_k^2}} \right] \right)^T \tag{7}$$

is the measurement function. The instrument noise vector $\boldsymbol{n}_k = [n_k^r, n_k^b, n_k^{\dot{r}}]^T$ is assumed to be Gaussian with zero-mean and covariance matrix

$$\boldsymbol{R}_k = \begin{bmatrix} \sigma_r^2 & 0 & \rho\sigma_r\sigma_{\dot{r}} \\ 0 & \sigma_b^2 & 0 \\ \rho\sigma_r\sigma_{\dot{r}} & 0 & \sigma_{\dot{r}}^2 \end{bmatrix}. \tag{8}$$

In the literature, n_k^r, n_k^b, and $n_k^{\dot{r}}$ are all assumed to be statistically independent, except for n_k^r and $n_k^{\dot{r}}$, which are correlated with a correlation coefficient ρ. In [34], it is computed when the range-Doppler offset is compensated.

B. MTT Procedure

The MTT procedure adopted in this paper is based on the JPDA paradigm, which is a Bayesian approach that associates all the validated measurements to the tracks by probabilistic weights. The track management is instead based on the popular M/N logic [15]. The filtering stage is performed using the UKF [29].

Assume that, at time k, a set of tracks are active/preliminary $\mathcal{T}_k = \{T_1(k), T_2(k), \ldots, T_J(k)\}$, where $T_j(k)$ is a natural number defining the identifier of the jth track. A validation gate region $\mathcal{G}_j(k)$, for all $j = 1, 2, \ldots, |\mathcal{T}_k|$, is constructed. Given that the target-originated measurements are Gaussian

distributed around the predicted measurement $z^j_{k|k-1}$ of target j, the gate is given by [15]

$$\mathcal{G}_j(k) = \left\{ z : \left(z - z^j_{k|k-1}\right)^T \left(S^j_k\right)^{-1} \left(z - z^j_{k|k-1}\right) < \gamma \right\} \tag{9}$$

where S^j_k is the innovation covariance, while the threshold γ determines the gating probability P_G, which is the probability that a measurement originated by target j is correctly validated.

1) Track Management: The track management is divided into the following steps.

1) *Track initiation*
   a) A measurement is associated to the track $T_j(k)$ if it falls in its gate region. Every unassociated measurement is called *initiator* and yields a *tentative track*.
   b) At the time following the detection of an initiator, a gate is set up. If a detection falls in the gate, this track becomes a *preliminary track*; otherwise, it is dropped.
   c) For each preliminary track, the JPDA-UKF can be initialized and used to set up a gate for the next sampling time.
   d) Starting from the third scan, a logic of M detections out of N scans is used for the subsequent gates.
   e) If, at the end (scan $N+2$), the logic requirement is satisfied, the track becomes a *confirmed* or *active track*; otherwise, it is discarded.
2) *Track termination*
   A confirmed track is terminated if one of the following conditions is verified.
   a) No detections have been validated in the past N^* most recent sampling times.
   b) The target's track uncertainty, evaluated from its covariance matrix, has grown beyond a given threshold.
   c) The target has reached an unfeasible maximum velocity v_{max}.
3) *Track update*
   a) For each active and preliminary track, the target state is updated applying the JPDA-UKF rule as described in Algorithm 1.

Algorithm 1 JPDA-UKF

- Update step.
  — At time index k, the validate measurements for the track j are $\boldsymbol{Z}^j_k = \{z^j_k(i)\}_{i=1}^{m_j(k)}$, where $m_j(k)$ is the cardinality of $\boldsymbol{Z}^j_k$. Compute the association probabilities, as indicated in [15], [18]

$$\beta_{ij} \triangleq \begin{cases} P\{\text{no meas. are originated by } j\text{th targ.}\}, & i = 0, \\ P\{i\text{th meas. is originated by } j\text{th targ.}\}, & i \neq 0. \end{cases} \tag{10}$$

  — Compute the state vector $\boldsymbol{x}^j_{k|k}$ and its covariance matrix $\boldsymbol{P}^j_{k|k}$

$$\boldsymbol{x}^j_{k|k} = \beta_{0j}\boldsymbol{x}^j_{k|k-1} + \sum_{i=1}^{m_j(k)} \beta_{ij}\boldsymbol{x}^j_{k|k}(i),$$

$$\boldsymbol{P}^j_{k|k} = \beta_{0j}\boldsymbol{P}^j_{k|k-1} + \sum_{i=1}^{m_j(k)} \beta_{ij} \cdot \left[\boldsymbol{P}^j_{k|k} + \left(\boldsymbol{x}^j_{k|k}(i) - \boldsymbol{x}^j_{k|k}\right)\left(\boldsymbol{x}^j_{k|k}(i) - \boldsymbol{x}^j_{k|k}\right)^T\right] \tag{11}$$

  where $\boldsymbol{x}^j_{k|k-1}$ is the state prediction and $\boldsymbol{x}^j_{k|k}(i)$ is the UKF update using the ith validated measurement $\boldsymbol{z}^j_k(i)$.
- Prediction step.
  — Compute the predicted state vector $\boldsymbol{x}^j_{k+1|k}$ and its covariance matrix $\boldsymbol{P}^j_{k+1|k}$ using the UKF (see Algorithm 2).

2) Target State Prediction and Update: The target state is updated accordingly to the measurement-to-track association rule of the JPDA-UKF, while the target state prediction follows directly from the motion model.

1) *Data association*
   a) A validation matrix is set up for all the confirmed and preliminary targets. Rows and columns of this matrix are indicized with all the validated measurements falling in the gate, plus the case of no measurements at all.
   b) From the validation matrix, all the feasible joint association events are constructed, according to the following two hypotheses: 1) A measurement is originated from one target; otherwise, it is a false alarm; and 2) each target generates, at most, one measurement, with detection probability P_D.
   c) The probabilities of the joint events are evaluated assuming the following: 1) Target-originated measurements are Gaussian distributed around the predicted location of the corresponding target measurement, and 2) false alarms are distributed in the surveillance region according to a Poisson point process of parameter λ, which represents the clutter density, assumed uniformly distributed in the gating region.
   d) The association probabilities of target j with measurement i, namely, β_{ij}, are obtained from the joint association probabilities (see details in [15] and [18]).
2) *Update and prediction*
   a) The target state $\boldsymbol{x}^j_{k|k}$ and its covariance $\boldsymbol{P}^j_{k|k}$ are then updated by averaging the UKF updates with the association probabilities β_{ij}.
   b) The predicted state $\boldsymbol{x}^j_{k+1|k}$ and its covariance $\boldsymbol{P}^j_{k+1|k}$ are obtained using Algorithm 2.

C. DF Procedure

The DF strategy applied to the HFSW radars is based on the T2T paradigm. This latter is constituted of two steps: the T2T *association* (T2T-A) and the T2T *fusion* (T2T-F) [15]. The T2T-A is a procedure which associates the tracks of the first

sensor, for example, Palmaria, to those of the second one, i.e., San Rossore. Let us assume that just a single track is active at each radar site: $\boldsymbol{x}_{k|k}^{P,i}$ at the Palmaria site and $\boldsymbol{x}_{k|k}^{R,j}$ at the San Rossore site. The true target states are respectively $\boldsymbol{x}_k^i$ and $\boldsymbol{x}_k^j$ for Palmaria and San Rossore. Let us define

$$\widehat{\Delta}_k^{ij} \triangleq \boldsymbol{x}_{k|k}^{P,i} - \boldsymbol{x}_{k|k}^{R,j}, \quad \Delta_k^{ij} \triangleq \boldsymbol{x}_k^i - \boldsymbol{x}_k^j. \tag{12}$$

The *same target* and *different target* hypotheses, namely, $\mathcal{H}_{ij}$ and $\bar{\mathcal{H}}_{ij}$, are formulated as

$$\mathcal{H}_{ij} : \Delta_k^{ij} = 0, \quad \bar{\mathcal{H}}_{ij} : \Delta_k^{ij} \neq 0. \tag{13}$$

The error in the difference of the state estimates is defined as

$$\widetilde{\Delta}_k^{ij} = \Delta_k^{ij} - \widehat{\Delta}_k^{ij} \tag{14}$$

with covariance, under the independence assumption,[1] given by

$$\mathbf{T}_k^{ij} = \boldsymbol{P}_k^i + \boldsymbol{P}_k^j. \tag{15}$$

The decision is based on the testing rule

$$D_{ij} \triangleq \left(\widehat{\Delta}_k^{ij}\right)^T \left[\mathbf{T}_k^{ij}\right]^{-1} \widehat{\Delta}_k^{ij} \underset{<}{\overset{\mathcal{H}_{ij}}{\geq}} D_\alpha \tag{16}$$

where the threshold D_α is computed such that $P\{D_{ij} > D_\alpha | H_{ij}\} = \alpha$. Exploiting the Gaussian assumption, the threshold corresponds to the $1-\alpha$ point of the chi-square distribution.

Considering that HFSW radars operate in a high vessel traffic region, it is common for both radar systems to have multiple track objects. Therefore, the previous testing rule must be extended as follows. Assume that Palmaria and San Rossore radars have a set of active/preliminary tracks $\mathcal{T}_k^P$, with $N_P = |\mathcal{T}_k^P|$, and $\mathcal{T}_k^R$, with $N_R = |\mathcal{T}_k^R|$, respectively. We define the binary assignment variable δ_{ij}, which is unitary if the track i of Palmaria is associated with the track j of San Rossore and null if otherwise. The list of tracks at each site is augmented with a dummy element, indicated with the null index,[2] to incorporate the case in which the track of one radar should be not associated with any of the tracks of the other radar. If we assume that the track association events among different track pairs are independent, then the 2-D assignment formulation finds the most likely (joint) track-to-track association hypothesis by solving the following constrained optimization [15]:

$$\begin{aligned} &\min_{\delta_{ij}} \textstyle\sum_{i=0}^{N_P} \sum_{j=0}^{N_R} \delta_{ij} c_{ij} \\ \text{s.t.} \quad &\textstyle\sum_{j=0}^{N_R} \delta_{ij} = 1,\ i = 1, \ldots, N_R, \\ &\textstyle\sum_{i=0}^{N_P} \delta_{ij} = 1,\ j = 1, \ldots, N_P, \\ &\delta_{ij} \in \{0,1\},\ 0 = 1, \ldots, N_R,\ j = 0, \ldots, N_P, \end{aligned} \tag{17}$$

where

$$c_{ij} = -\ln \mathcal{L}_{ij}. \tag{18}$$

[1]Note that the track estimates $\boldsymbol{x}_{k|k}^{P,i}$ and $\boldsymbol{x}_{k|k}^{R,i}$ are not independent [15]. However, in this paper, we use this simplification since the procedure to carry out the dependence would require a higher computational load.

[2]For instance, δ_{i0} represents the case that the track i is not associated.

For $i, j \geq 1$, $\mathcal{L}_{ij}$ is the likelihood ratio of the two tracks being from the same target versus being from two different targets and is proportional to D_{ij}. For $i = 0$ (or $j = 0$), $\mathcal{L}_{ij}$ is the likelihood ratio of an incomplete assignment (see further details in [15]). The optimization problem of (17) can be solved using standard procedures, e.g., the auction algorithm, Jonker-Volgenant-Castanon (JVC) assignment algorithm, and linear programming by relaxing the integer constraint. Defining δ_{ij}^* as the T2T-A pairs, the fusion target state is computed for all the associated tracks, $\delta_{ij}^* = 1$, $i, j \geq 1$. It has higher accuracy than the individual state estimates. For all the unassociated tracks, the fusion system is equivalent to the single sensor, i.e., an *OR* fusion strategy is applied. The output of the DF system is then a list of tracks $\mathcal{T}_k^F$ whose cardinality is not larger than $N_P + N_R$. The track initiation and termination are dependent on the track management at the local sensor. The tracks at the fusion system survive if at least one of its parents is not deleted. The JPDA-UKF and the T2T-A/F procedures are summarized by Algorithms 1, 2, and 3, respectively.

Algorithm 2 UKF

- Prediction step.
  - Define the sigma-point matrix $\boldsymbol{\chi}_{k-1|k-1}^j$ at time $k-1$ for the track j at $k-1$

$$\begin{aligned} \boldsymbol{\chi}_{k-1|k-1}^j &= \left[\boldsymbol{\chi}_{k-1|k-1}^j(0), \ldots, \boldsymbol{\chi}_{k-1|k-1}^j(2n_x)\right] \\ &= \left[\boldsymbol{x}_{k-1|k-1}^j, \boldsymbol{X}_{k-1|k-1}^j + \widetilde{\boldsymbol{P}}_{k-1|k-1}^j, \right. \\ &\qquad \left. \boldsymbol{X}_{k-1|k-1}^j - \widetilde{\boldsymbol{P}}_{k-1|k-1}^j\right] \end{aligned} \tag{19}$$

    where $\widetilde{\boldsymbol{P}}_{k-1|k-1}^j = \sqrt{(n_x + \varsigma)\boldsymbol{P}_{k-1|k-1}^j}$ is the Cholesky factorization of the scaled state covariance matrix, ς is a scaling parameter, and $\boldsymbol{X}_{k-1|k-1}^j$ is the $n_x \times n_x$ matrix whose columns are all equal to $\boldsymbol{x}_{k-1|k-1}^j$.
  - Propagate sigma-point matrix $\boldsymbol{\chi}_{k|k-1}^j$, according to (3), and write it as in (19).
  - Predict state vector $\boldsymbol{x}_{k|k-1}^j$ and its covariance $\boldsymbol{P}_{k|k-1}^j$ using the unscented weights w_n

$$\begin{aligned} \boldsymbol{x}_{k|k-1}^j &= \sum_{n=0}^{2n_x} w_n \widetilde{\boldsymbol{\chi}}_{k|k-1}^j(n), \\ \boldsymbol{P}_{k|k-1}^j &= \boldsymbol{Q}_k + \sum_{n=0}^{2n_x} w_n \left(\widetilde{\boldsymbol{\chi}}_{k|k-1}^j(n) - \boldsymbol{x}_{k|k-1}^j\right) \\ &\quad \cdot \left(\widetilde{\boldsymbol{\chi}}_{k|k-1}^j(n) - \boldsymbol{x}_{k|k-1}^j\right)^T. \end{aligned} \tag{20}$$

  - Predict sigma-point matrix $\boldsymbol{\chi}_{k|k-1}^j$, and write it as in (19). Predict observation matrix $\boldsymbol{\gamma}_{k|k-1}^j$ using (6), and write it as in (19).

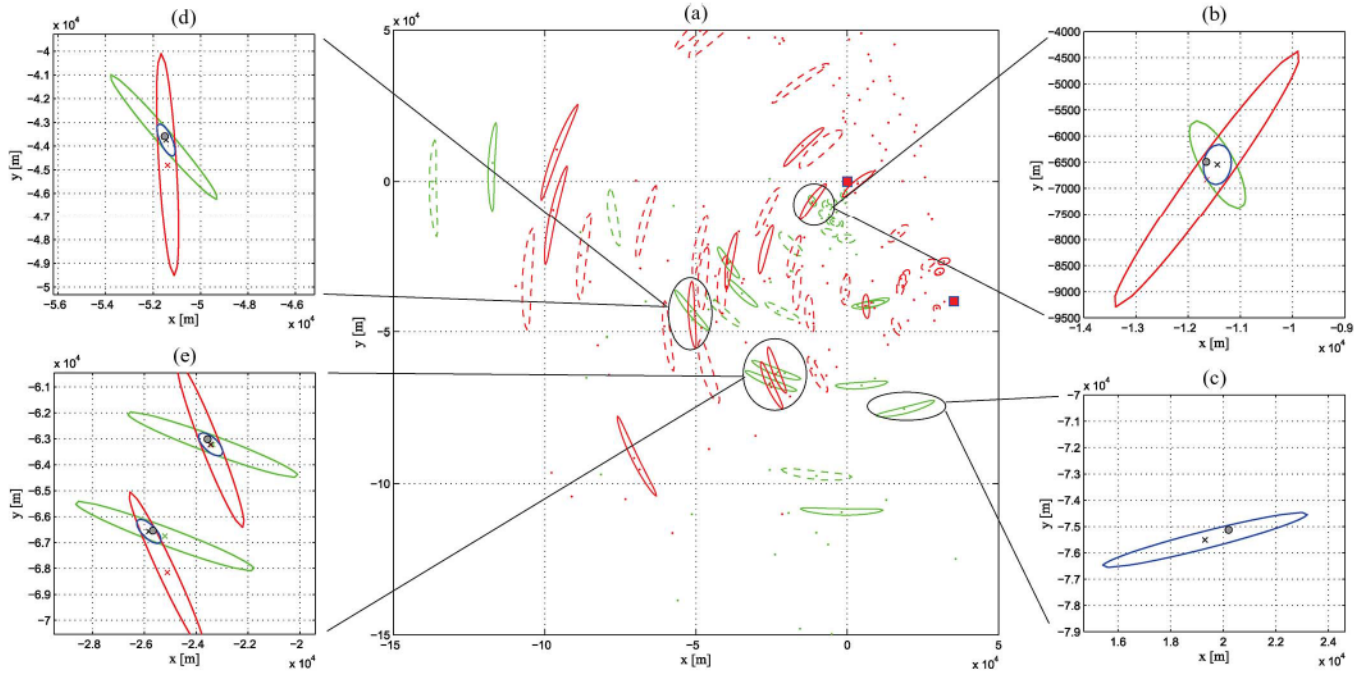

Fig. 3. Example of the MTT-DF system procedure at a given time scan. (a) Main central plot, (square) radar location, validation gates of (solid line) confirmed and (dash line) preliminary tracks, projected in the Cartesian plane, and (dots) OS-CFAR detections of the radar in (green) Palmaria and (red) San Rossore. Plot (b)-(c)-(d)-(e) with state estimates and related covariances of confirmed tracks: (Green) JPDA-UKF at Palmaria, (red) JPDA-UKF at San Rossore, (black) T2T-A/F, and (blue) AIS reports.

— Predict observation vector $z^j_{k|k-1}$ and its covariance S^j_k

$$z^j_{k|k-1} = \sum_{n=0}^{2n_x} w_n \gamma^j_{k|k-1}(n),$$

$$S^j_k = R_k + \sum_{n=0}^{2n_x} w_n \left(\gamma^j_{k|k-1}(n) - z^j_{k|k-1}\right) \cdot \left(\gamma^j_{k|k-1}(n) - z^j_{k|k-1}\right)^T. \quad (21)$$

- Update step.
  — Compute the filter gain $W^j_k = \sum_{n=0}^{2n_x} w_n (\chi^j_{k|k-1}(n) - x^j_{k|k-1}) \cdot (\gamma^j_{k|k-1}(n) - z^j_{k|k-1})^T (S^j_k)^{-1}$.
  — Compute the state vector $x^j_{k|k}(i)$ and its covariance matrix $P^j_{k|k}$ based on the ith associated measurement $z^j_k(i)$ to the jth track

$$x^j_{k|k}(i) = x^j_{k|k-1} + W^j_k \left(z^j_k(i) - z^j_{k|k-1}\right),$$
$$P^j_{k|k} = P^j_{k|k-1} - W^j_k S^j_k \left(W^j_k\right)^T. \quad (22)$$

D. Snapshot of the MTT-DF Working on Palmaria and San Rossore Sites

In Fig. 3, the main features of the MTT-DF system are represented for a given timestamp. In the main central plot, we depict the radar picture (dots) and the validation gating region, projected in the Cartesian plane, of the preliminary and active tracks (dashed and solid lines, respectively). It has to be noted that, in the spherical domain, the validation gate has an elliptical shape, while when projected into the Cartesian plane, it has a kind of *banana* shape (see also [29]).

In the lateral plots, there are some examples of associated and fused tracks, where the target position estimates and their related covariances are depicted with the AIS reports. In panel (b)-(d)-(e), we have four targets, detected from both radars. It is worth noting that the fusion strategy improves the accuracy of the target position estimate and reduces its uncertainty. Furthermore, panel (c) shows the event in which only one radar detects the target. In this case, the fusion output coincides with the single-radar output. This latter example explains the improvement, in terms of ToT, of the fusion scheme. However, many radar detections are not going to be confirmed as active tracks by the tracking logic, leading to an improvement of the FAR. The quantitative analysis of the cases, presented in Fig. 3, is reported in Section V.

IV. Performance Assessment

In this section, we describe the procedure for assessing the performance of the target detection, tracking, and fusion algorithms. Ships and vessels exceeding a given gross tonnage[3] are equipped with AIS transponders for position reporting, as established by the International Convention for the "Safety of Life at Sea" (SOLAS), 1974 Convention [35]. Ships repeatedly broadcast their name, position, and other details for automatic display on nearby ships. While this allows ships to be aware and

[3]The AIS is required for all the ships exceeding 300 gross tonnage and engaged on international voyages, for all cargo ships of 500 gross tonnage and not engaged on international voyages, and for all passenger ships. On average, a gross weight of 300 tons corresponds to a length of about 25 m.

keep track of other ships in their immediate vicinity, coastal states will also be able to receive, plot, and log the data by means of base stations along the coast. AIS reports contain both dynamic information (e.g., latitude, longitude, course over ground (COG), speed over ground (SOG), and time) and static information (e.g., vessel type and dimension information). In this paper, given that the AIS information has a GPS accuracy, the static and kinematic AIS data are used as ground-truth data.

Even if it is well known that some vessels are not cooperative, here, any estimated track, with no corresponding AIS, is considered as false. We also suppose that the information transmitted by ships is not corrupted by any errors (intentional or unintentional). Note that AIS reports are not synchronized with radar scans; however, they are more frequent. This means that, when they are filtered and interpolated on the HFSW radar timestamps, we introduce no degradation in terms of accuracy, and they can still be considered ground-truth data.

A. AIS Data

The AIS report represents the set of the target state vectors at time k

$$\mathcal{X}_k^{AIS} \triangleq \{\boldsymbol{x}_k^n\}_{n\in\mathcal{N}_k} \tag{23}$$

where $\mathcal{N}_k$ is the list of ships reporting their static and kinematic information in the recording interval. In this phase, longitude, latitude, COG, and SOG information is converted to obtain the current Cartesian data vector. Each AIS data vector is filtered and interpolated at the radar timestamps t_k. As said, linear interpolation is accurate because of the high data rate of the AIS with respect to the radar. However, it is possible that no AIS information from the vessel is received for a long period of time. In this case, the interpolated route could not represent the ground truth anymore. In order to eliminate these cases, we define the following flag index:

$$I_m^n = \begin{cases} 1, & \Delta T_m^n \leq \Delta T_{max} \\ 0, & \text{otherwise,} \end{cases} \tag{24}$$

where m represents the time instant τ_m^n at which the nth ship transmits its position and $\Delta T_m^n = \tau_m^n - \tau_{m-1}^n$ is the time interval between two AIS transmissions of the nth vessel. The parameter ΔT_{max} represents the maximum acceptable time from the last report. In the time interval when $I_m^n = 0$, the AIS data from the nth vessel are not considered as ground truth and consequently not used for the performance evaluation.

B. HFSW Radar Data

The detections (e.g., OS-CFAR) and the tracks (e.g., JPDA-UKF and T2T-A/F), constituting the HFSW radar data set, are the target state estimates at time k

$$\mathcal{X}_k^{HFSW} \triangleq \left\{\boldsymbol{x}_k^j\right\}_{j\in\mathcal{T}_k} \tag{25}$$

where $\mathcal{T}_k$ is the set of detections for the OS-CFAR or the set of confirmed tracks for the JPDA-UKF and T2T-A/F at the time step k.

An association procedure between the AIS and the radar data is required to compute the system performance. This association is evaluated on each daily data set for the OS-CFAR detector at Palmaria and San Rossore, for the JPDA-UKF tracker at Palmaria and San Rossore, and for the T2T-A/F system. At time k, each AIS contact $\bar{\boldsymbol{x}}_k^n \in \mathcal{X}_k^{AIS}$, with $n \in \mathcal{N}_k$, is associated to a single track contact $\hat{\boldsymbol{x}}_k^j \in \mathcal{X}_k^{HFSW}$, with $j \in \mathcal{T}_k$. The association is carried out by searching the nearest among all the HFSW radar reports falling inside a 3-D (range, azimuth, and range rate) *performance validation region* (PVR) centered on the AIS contact

$$(\mathcal{T}_k \ni j \to n \in \mathcal{N}_k) : d\left(\hat{\boldsymbol{x}}_k^j, \bar{\boldsymbol{x}}_k^n\right) = \min_{i\in\mathcal{T}_k} d\left(\hat{\boldsymbol{x}}_k^i, \bar{\boldsymbol{x}}_k^n\right). \tag{26}$$

The jth radar contact is validated if this distance is below a given threshold. If the nth AIS report has a validated track contact, we have a *correct detection*; otherwise, we have a *missed detection*. At each time, the AIS report can be associated with, at most, one radar report. All the other radar contacts, which are not validated, are considered *false alarms*.

Algorithm 3 T2T-A/F

- Association step.
  - At time step k, solve the optimization problem (17), obtaining the association matrix $\{\Delta^*\}_{ij} = \delta_{ij}^*$.
- Fusion step.
  - For all the associated pairs (i, j), with $\delta_{ij}^* = 1$, compute the fused target state estimate and its covariance

$$\begin{aligned} \boldsymbol{x}_{k|k}^{F,ij} = {} & \boldsymbol{P}_{k|k}^{R,j}\left(\boldsymbol{P}_{k|k}^{P,i} + \boldsymbol{P}_{k|k}^{R,j}\right)^{-1}\boldsymbol{x}_{k|k}^{P,i} \\ & + \boldsymbol{P}_{k|k}^{P,i}\left(\boldsymbol{P}_{k|k}^{P,i} + \boldsymbol{P}_{k|k}^{R,j}\right)^{-1}\boldsymbol{x}_{k|k}^{R,j}. \end{aligned} \tag{27}$$

$$\boldsymbol{P}_{k|k}^{F,ij} = \boldsymbol{P}_{k|k}^{P,i}\left(\boldsymbol{P}_{k|k}^{P,i} + \boldsymbol{P}_{k|k}^{R,j}\right)^{-1}\boldsymbol{P}_{k|k}^{R,j}. \tag{28}$$

  - For all the unassociated tracks, i.e., $\delta_{ij}^* = 1$ with $i = 0$ or $j = 0$, the fused track is equal to the track at the single sensor.

C. Performance Metrics

1) ToT and FAR: The ToT is defined as the ratio between the time during which the tracker follows the target and the whole interpolated ship route. The FAR is defined as the number of false track/detection contacts, normalized by the recording time interval and the area of the surveyed region. An ideal system would have a ToT $= 100\%$ with no false alarms. Clearly a tradeoff is present between ToT and FAR, like in the receiver operating characteristic of a statistical hypothesis test problem.

TABLE I
MTT PARAMETERS

Parameter	*Value*	*Specification*
T_k	16.64 s/33.28 s	Sampling period
σ_v	$1 \cdot 10^{-2}\,\mathrm{m\,s^{-2}}$	Process noise
σ_r	150 m	Std range
σ_b	1.5°	Std bearing
$\sigma_{\dot{r}}$	$0.1\,\mathrm{m\,s^{-1}}$	Std Range-rate
P_D	0.35	Detection probability
λ	$10^{-9}\,\mathrm{m^{-2}}$	Clutter density
γ	3.3^2	Gate threshold
$\sigma_{x,y}$	500 m	Init. filter (pos.)
$\sigma_{\dot{x},\dot{y}}$	$10\,\mathrm{m\,s^{-1}}$	Init. filter (vel.)
v_{max}	$25\,\mathrm{m\,s^{-1}}$	Maximum velocity
M/N	7/8	Track initiation logic
N^*	3	Track termination logic

TABLE II
PERFORMANCE ASSESSMENT PROCEDURE PARAMETERS

Parameter	*Value*	*Specification*
Δr	1.5 km	PVR range threshold
Δb	2°	PVR bearing threshold
$\Delta \dot{r}$	$2\,\mathrm{m\,s^{-1}}$	PVR range-rate threshold
ΔT_{max}	30 s	Maximum time for AIS flag

In fact, decreasing the detection threshold of the OS-CFAR algorithm, we increase both the ToT and the FAR.

2) RMSE: The accuracy of the radar system is evaluated in terms of RMSE and represents the localization capacity of a detected target.

3) TF Analysis: The track fragmentation is defined by the pair ToT and number of radar tracks N^{TF} associated with a single target. An ideal system would have ToT $= 100\%$ with $N^{TF} = 1$, i.e., the radar system is able to follow the target along its whole route without losing the track. Typically, we have instead that ToT $< 100\%$ and $N^{TF} > 1$. The TF depends on different aspects, including the target size, geometry target-radar location, sea clutter, and interferences.

V. EXPERIMENTAL RESULTS

The OS-CFAR, JPDA-UKF, and T2T-A/F procedures are tested on a 25-day data set collected between May 8 and June 4, 2009. The analysis is performed only in the region where the two radar fields of view overlap, namely, the *fusion region*. In this way, it is possible to observe the same ship routes and to provide a fair comparison between the single radars and the fusion system. In this region, the average number of AIS-carrying vessels per day varied between 59 (May 18) and 91 (May 26). The parameters used in the MTT algorithms are summarized in Table I, while the parameters used for performance assessment are given in Table II.

A. Analysis of True Tracks

A sample scenario is depicted in Fig. 4. In this day (i.e., May 8), 87 AIS-carrying ships were recorded. The ship trajectories and the true active tracks are displayed as follows. The output tracks of the T2T-A/F and the AIS ship routes are depicted in the surveyed area with the blue and black lines, respectively. The two JPDA-UKFs, Palmaria (green) and San Rossore (red), are reported as well. There is a quite good

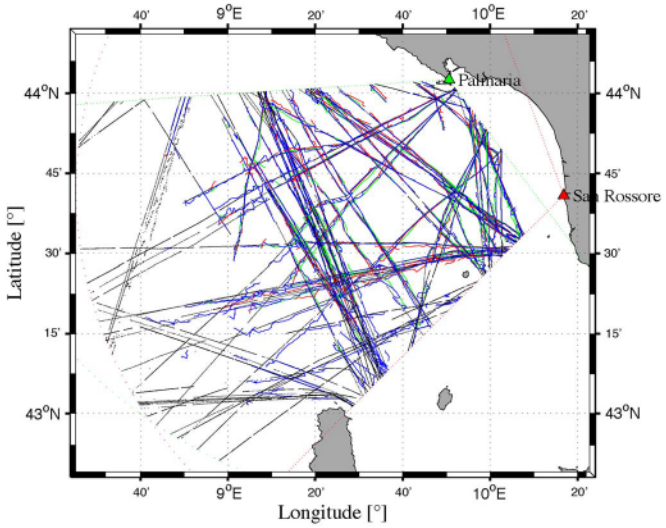

Fig. 4. True active tracks in the fusion region on May 8, 2009: (Black) AIS, (green) Palmaria, (red) San Rossore, and (blue) T2T-A/F.

agreement with the AIS ship routes. Unfortunately, the tracking capabilities of the three systems significantly degrade after a 100 km distance and at the edges of the 120° area covered by each sensor. This problem can be partially explained by the presence of land scatter (e.g., the northern part of Corsica), not perfectly filtered out by the beamforming algorithm.

B. ToT Analysis

The ToT, averaged over 25 days, is presented in Fig. 5 at the varying of range, azimuth, and range rate and in Fig. 6 at the varying of ship length. The ToT versus range is shown in Fig. 5(a) and (d), w.r.t. Palmaria and San Rossore, respectively, and is estimated over 10 km distance intervals, considering all the azimuth angles and range-rate values. The peak values at Palmaria occur in the 10–50 km interval, where the ToT is about 65%–77% for the JPDA-UKF (green) and 49%–58% for the OS-CFAR algorithm (red), while it is about 80%–90% for the T2T-A/F strategy (blue). The maximum improvement of the JPDA-UKF w.r.t. the OS-CFAR is 20%, while it is 15% for the T2T-A/F w.r.t. the JPDA-UKF. Beyond the 80 km limit, the T2T-A/F relies almost completely on the JPDA-UKF output of Palmaria. Performance rapidly decreases, and the differences among the curves become negligible.

For San Rossore, the peak value is instead about 55%–57%, for both the tracker and the detector. However, on average, the OS-CFAR achieves better performance than the JPDA-UKF. Since the two sensors share the same setup parameters and observe the same vessels, a possible reason can be found in the relative geometry between the ship routes and the sensor positions, supposedly more favorable at Palmaria than at San Rossore. For completeness, no AIS reports were available in the first 10 km from San Rossore. Finally, the DF strategy leads to a final ToT value of 79%, with a maximum improvement of about 30% w.r.t. the JPDA-UKF.

It is interesting to observe that the gain of the T2T-A/F system w.r.t. San Rossore is larger than w.r.t. Palmaria (i.e., about 10%–15% and 15%–30% in the 0–80 km interval w.r.t.

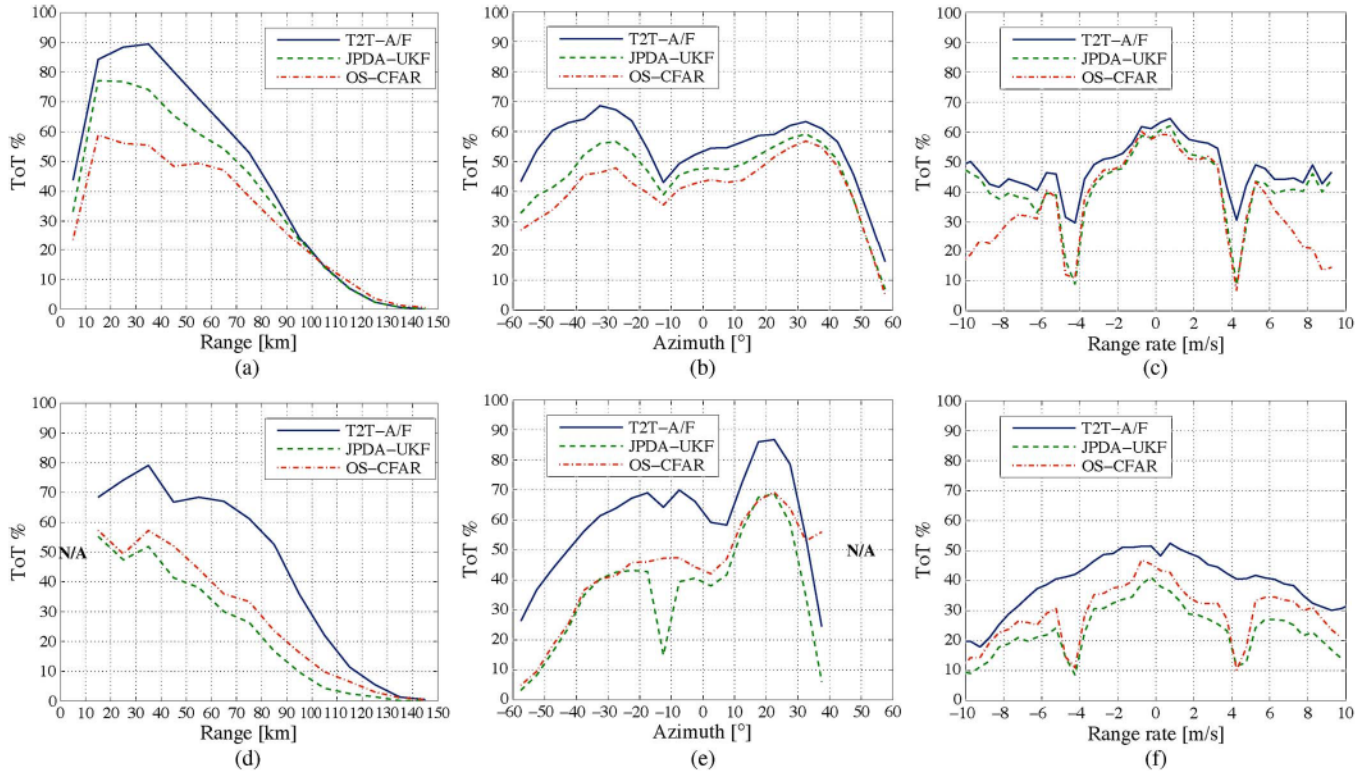

Fig. 5. Estimated ToT percent versus range [km], azimuth [°], and range rate [m/s], w.r.t. (upper plots) Palmaria and (lower plots) San Rossore sites: (Blue) T2T-A/F, (green) JPDA-UKF, and (red) OS-CFAR. (a) ToT versus range w.r.t. Palmaria. (b) ToT versus azimuth w.r.t. Palmaria. (c) ToT versus range rate w.r.t. Palmaria. (d) ToT versus range w.r.t. San Rossore. (e) ToT versus azimuth w.r.t. San Rossore. (f) ToT versus range rate w.r.t. San Rossore.

Palmaria and San Rossore, respectively). This is a proof that the Palmaria setup performs better than that of San Rossore and, hence, the T2T-A/F relies mostly on the former sensor. Aspect diversity provides more information, but the improvement of the detection capabilities comes at the cost of an increase of the FAR, as it will be discussed in Section V-C.

The ToT versus azimuth is estimated over 5°-wide angular intervals and averaged over all the surveyed range and range-rate intervals. At Palmaria, two local peaks can be observed, i.e., the first one is between $-35°$ and $-25°$ w.r.t. the array broadside direction, while the second one is between 30° and 40° [see Fig. 5(b)]. For angles close to the limits of the surveyed area, i.e., around $\pm 60°$, the ToT strongly diminishes. The T2T-A/F achieves, on average, a larger ToT than the JPDA-UKF. This is especially true for those angles smaller than $-15°$, for which the gain is about 10%–20%.

At San Rossore, the peak values concentrate between 10° and 35°, i.e., the region in front of the Gulf of La Spezia. Anyway, the area covered by San Rossore is limited between $-60°$ and 40°. In this interval, the values vary between 50% and 68% for both the JPDA-UKF and the OS-CFAR algorithms. A strong degradation of the performance can be observed at the borders of the surveyed region, i.e., for those angles close to $-60°$. The OS-CFAR output grants results comparable with that of the JPDA-UKF, except for the regions close to 40° and $-15°$ [see Fig. 5(e)]. The reasons of such a behavior are currently under investigation. Finally, the gain obtained using the T2T-A/F strategy is almost constant and varies between 15% and 25% [see Fig. 5(e)].

The ToT versus range rate, evaluated over 0.5 m/s speed intervals and averaged over the whole defined range and azimuth intervals, is depicted in Fig. 5(c) and (f), for Palmaria and San Rossore, respectively. Observing the two JPDA-UKFs, Palmaria (a) exhibits a larger ToT than San Rossore (b), with a maximum value of about 62% compared to about 45%. At both sites, the largest values are given for radial speeds comprised between the two first-order Bragg velocities (e.g., for a carrier frequency of 12.50 MHz, these are about ± 4.32 m/s). In fact, as the ship gets closer the zero-Doppler (i.e., it moves tangentially), it maximizes its radar cross section. Outside this interval, the ToT diminishes by about 10% on average, but sensibly more at San Rossore than at Palmaria. Moreover, the OS-CFAR ship detection performances degrade with increasing radial speed (in modulus) for Palmaria and slightly less for San Rossore. According to the CFAR rule, the detection threshold is chosen to keep the FAR constant. This means that, in the proximity of the Bragg scattering regions, the detection threshold is increased, thus decreasing the probability of detection. This issue does not concern only the detection algorithm but affects also the tracking procedure, due also to the strict track maintenance/termination logic (see Table I). On the contrary, the aspect diversity exploited by the track-fusion strategy allows to fix this issue, and the notches around ± 4.32 m/s are less significant. As expected, the T2T-A/F improvement is more pronounced w.r.t. San Rossore (i.e., about 30%) than w.r.t. Palmaria (i.e., about 20%).

In Fig. 6 the average ToT is estimated for ship length multiples of 50 m. Results are averaged over the defined range,

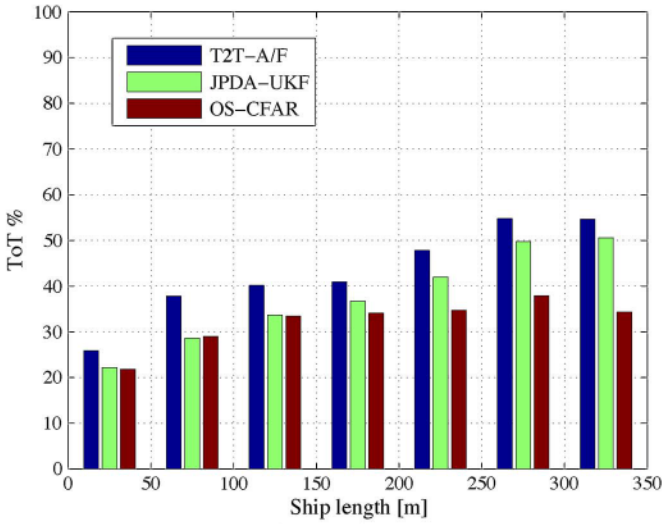

(a) ToT vs ship length w.r.t. Palmaria.

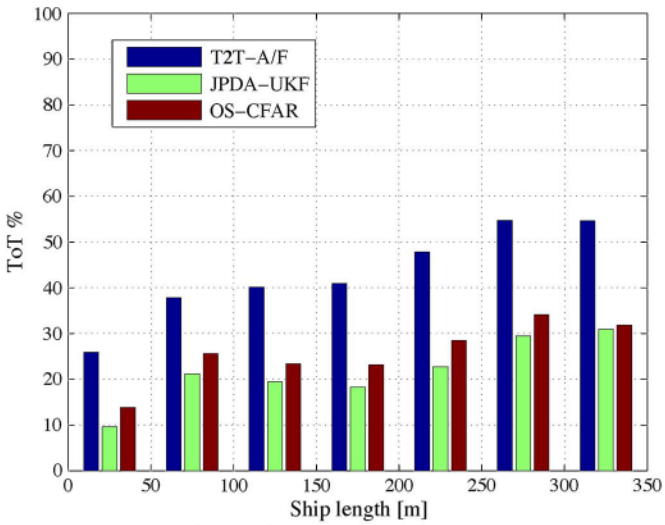

(b) ToT vs ship length w.r.t. San Rossore.

Fig. 6. Estimated ToT percent versus ship length [m], w.r.t. (a) Palmaria and (b) San Rossore sites: (Blue) T2T-A/F, (green) JPDA-UKF, and (red) OS-CFAR. (a) ToT versus ship length w.r.t. Palmaria. (b) ToT versus ship length w.r.t. San Rossore.

azimuth, and range-rate intervals and over the whole recording interval. As expected, an increase in the ship length brings an increase in the ToT. This is especially clear for huge ships (i.e., longer than 250 m), for which the ToT $= 55\%$. The DF strategy improves the ToT of about 5%–10% for Palmaria and 15%–25% for San Rossore on average. This result proves that the T2T-A/F output relies mainly on the JPDA-UKF at Palmaria than on the one at San Rossore. At Palmaria, the improvement of the JPDA-UKF w.r.t. the OS-CFAR seems to be related to very large ships (i.e., longer than 200 m) moving at high radial speed in modulus (i.e., $|\dot{r}| > 6$ m/s) up to an 80 km distance, as shown in Figs. 6(a) and 5(a) and (c), respectively. At San Rossore, the OS-CFAR performs better than the JPDA-UKF [see Fig. 6(b)]. This fact can be explained by the relative geometry of the ship routes, which seem to lead to more fragmented tracks. However, on average, we do not expect that the JPDA-UKF algorithm performs significantly better

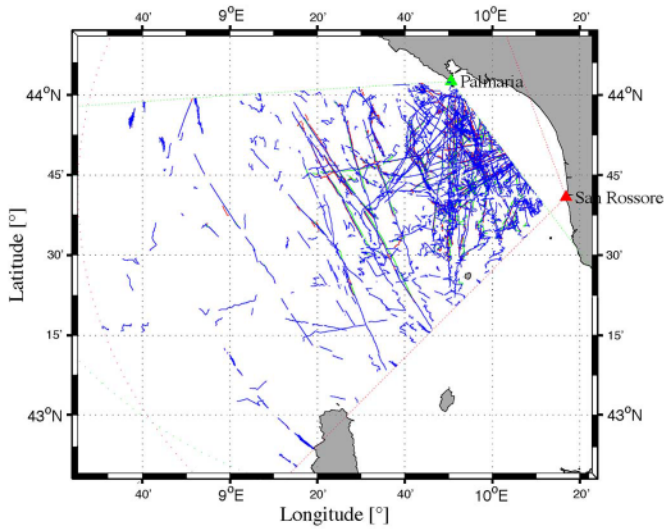

Fig. 7. False active tracks in the fusion region on May 8, 2009: (Green) Palmaria, (red) San Rossore, and (blue) T2T-A/F.

than the OS-CFAR, due to the strict rules for track initiation, maintenance, and termination (cf. Table I).

C. Analysis of False Tracks

Active false tracks recorded on May 8 are shown in Fig. 7. The color coding is the same as that used for the true tracks. A significant number of active false tracks can be observed, having a good time coherency but no associated AIS report. In fact, it is interesting to observe that some of these tracks closely follow the main ship routes observed in Fig. 4 and, at far distance, they exhibit a peculiar fragmented behavior, as it will be discussed in Section V-E.

In addition, a significant amount of false tracks crowds the sea in front of the coasts of Tuscany, Italy. It is possible that, in the surveyed area, a number of ships are not carrying any AIS transponder (e.g., fishing boats or military vessels) or are not cooperative. Moreover, it is interesting to observe the accumulations of radially moving tracks, distributed at long distances at the borders of the surveyed region. They are probably false tracks generated by land scattering returns.

D. FAR Analysis

The FAR analysis is carried out at the varying of range, azimuth, and range rate and averaged over all the days, on the same intervals considered for the ToT. On each specific interval, FAR values are normalized such that their weighted sum provides the total FAR per unit of time and area for that day.

The FAR versus range is shown in Fig. 8(a) and (d), for Palmaria and San Rossore, respectively. As expected, the application of the tracking algorithm significantly reduces the number of false track contacts and cancels most of clutter-originated returns (cf. green (JPDA-UKF) and red (OS-CFAR) lines), particularly at far distance. False detections manifest a more uniform behavior along range than the tracker outputs, which tend instead to accumulate in the first 80 km from the

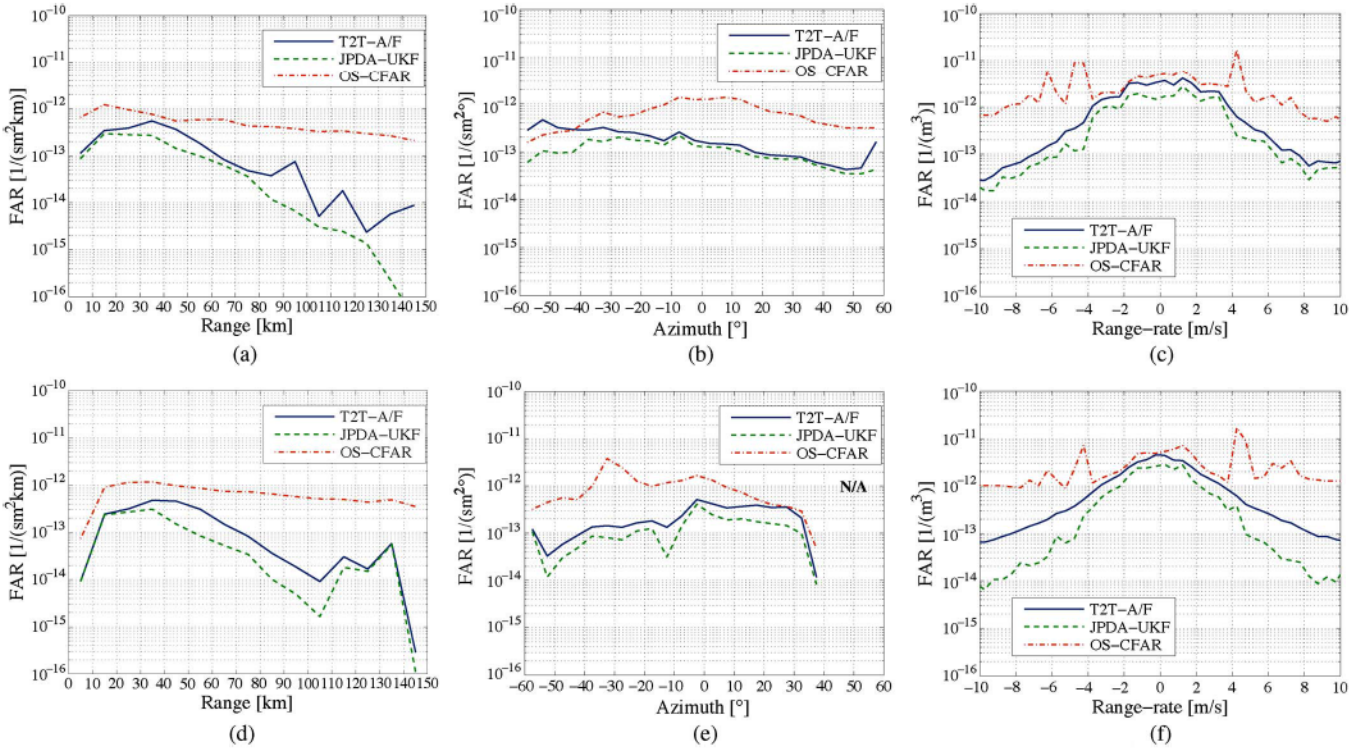

Fig. 8. Estimated FAR versus range [km], azimuth [°], and range rate [m/s], w.r.t. (upper plots) Palmaria and (lower plots) San Rossore sites: (Blue) T2T-A/F, (green) JPDA-UKF, and (red) OS-CFAR. (a) FAR versus range w.r.t. Palmaria. (b) FAR versus azimuth w.r.t. Palmaria. (c) FAR versus range rate w.r.t. Palmaria. (d) FAR versus range w.r.t. San Rossore. (e) FAR versus azimuth w.r.t. San Rossore. (f) FAR versus range rate w.r.t. San Rossore.

radars. This can be explained by referring to Fig. 7. Here, a significant number of suspicious false tracks can be observed in the proximity of the coast. The same behavior has been described also for ToT, as shown in Fig. 5(a) and (d). The proposed T2T-A/F strategy (blue) brings more false alarms but conversely grants also better ToT, as discussed in Section V-B. In fact, an active track is declared at the T2T-A/F system when at least one track is available at two sensors (i.e., *OR* fusion strategy).

The distribution of the false contacts versus azimuth is depicted in Fig. 8(b) and (e). At Palmaria, no significant differences arise from the analysis of the JPDA-UKF and T2T-A/F outputs, except for an increase at angles smaller than $-15°$. This is in agreement to what is shown also in Fig. 5(b). At San Rossore instead, the increase in the FAR is almost constant along azimuth. As expected, an increase in the ToT estimate corresponds to an increase in the FAR, as shown in Fig. 5(e).

The estimated FARs versus range rate are shown in Fig. 8(c) and (f), for Palmaria and San Rossore, respectively. A relevant amount of false contacts are produced by sea clutter, not perfectly filtered out by the OS-CFAR detection algorithm (red line). In fact, these contacts distribute along the most relevant harmonics of the wave spectrum (cf. Section II-B). As expected, the tracking algorithms prune most of these returns, and false track contacts accumulate mainly between the two Bragg-wave velocities, where most of the vessels lay.

As known, the FAR is related to the ToT, and statistically, an increase in the probability of detection bears an increase in the probability of false alarm. This evidence is shown in the joint analysis of Figs. 5 and 8 and manifests in the scatterplot

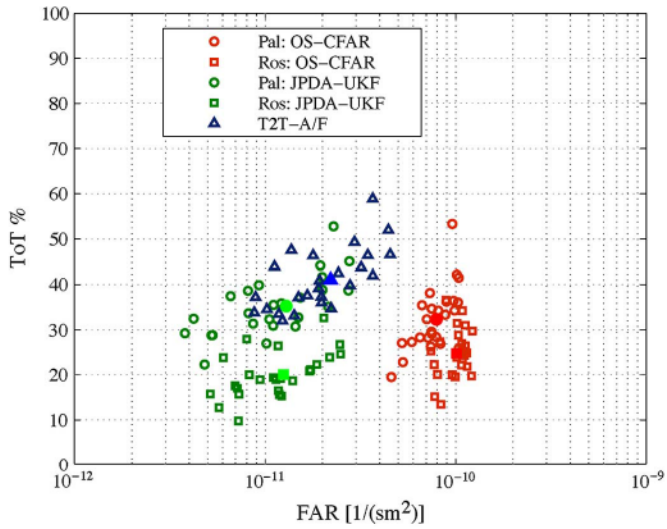

Fig. 9. ToT versus FAR scatterplot analysis: (Red circles) OS-CFAR at Palmaria, (red squares) OS-CFAR at San Rossore, (green circles) JPDA-UKF at Palmaria, (green squares) JPDA-UKF at San Rossore, and (blue triangles) T2T-A/F. Values for each day are represented by empty symbols, and averaged values are represented by full symbols.

analysis of Fig. 9. The red circles and squares represent the pairs (FAR and ToT) obtained by the OS-CFAR algorithms, at Palmaria and San Rossore, respectively. The green circles and squares represent instead the two JPDA-UKF outputs, while the blue triangles are the output pairs of the T2T-A/F system. As to be expected, in terms of ToT, the JPDA-UKF provides results comparable to those of the detection algorithm. However, most of the false alarms are pruned, and the FAR is about one order of

TABLE III
ToT Versus FAR, Average Values

Algorithm	*FAR* $[s^{-1}m^{-2}; hh^{-1}km^{-2}]$	*ToT* %
OS-CFAR at Palmaria	$(8 \cdot 10^{-11}; 0.288)$	32
OS-CFAR at S. Rossore	$(10 \cdot 10^{-11}; 0.360)$	25
JPDA-UKF at Palmaria	$(1.3 \cdot 10^{-11}; 0.047)$	35
JPDA-UKF at S. Rossore	$(1.2 \cdot 10^{-11}; 0.043)$	20
T2T-A/F	$(2.2 \cdot 10^{-11}; 0.079)$	41

TABLE IV
TF Statistics and Average ToT

Date	Palmaria		San Rossore		Fusion	
	$(\mu;\sigma)$	ToT	$(\mu;\sigma)$	ToT	$(\mu;\sigma)$	ToT
08/05	(4.0; 2.1)	53	(4.3; 2.3)	33	(4.7; 3.0)	59
09/05	(3.7; 2.5)	39	(3.9; 2.2)	28	(4.4; 3.0)	48
10/05	(3.7; 1.8)	29	(3.6; 2.0)	18	(4.2; 2.7)	35
11/05	(3.9; 2.5)	32	(3.8; 2.4)	19	(4.3; 2.7)	37
12/05	(3.9; 2.8)	27	(3.6; 2.3)	19	(4.7; 3.2)	36
13/05	(3.8; 2.2)	29	(3.3; 2.1)	17	(4.3; 2.5)	33
14/05	(3.3; 2.1)	22	(3.3; 2.0)	20	(4.4; 2.8)	32
15/05	(4.1; 2.3)	40	(3.9; 2.5)	26	(4.8; 2.9)	46
16/05	(3.9; 2.5)	34	(3.8; 3.1)	19	(4.3; 3.1)	37
17/05	(3.8; 2.6)	35	(3.7; 2.4)	17	(4.5; 3.2)	39
18/05	(3.9; 2.2)	35	(3.7; 2.0)	24	(4.4; 2.7)	42
19/05	(3.4; 2.4)	45	(3.5; 2.3)	27	(3.9; 2.8)	52
22/05	(4.2; 2.7)	44	(3.9; 2.4)	19	(5.0; 3.2)	49
23/05	(4.7; 2.7)	37	(3.9; 2.3)	24	(5.8; 3.7)	44
24/05	(3.7; 2.9)	36	(4.2; 2.3)	19	(4.7; 3.7)	41
25/05	(3.5; 2.5)	37	(4.0; 2.5)	25	(4.5; 2.9)	47
26/05	(4.1; 2.5)	42	(4.4; 2.5)	22	(4.9; 3.0)	46
28/05	(4.0; 3.2)	33	(3.2; 1.8)	24	(4.7; 3.7)	40
29/05	(5.0; 3.0)	39	(3.9; 2.0)	21	(5.6; 3.6)	44
30/05	(4.5; 2.7)	31	(3.6; 2.3)	15	(4.8; 3.5)	35
31/05	(4.1; 2.9)	32	(3.0; 1.9)	16	(4.6; 2.9)	37
01/06	(4.4; 3.1)	37	(3.2; 1.9)	16	(4.8; 3.4)	43
02/06	(3.7; 2.8)	31	(3.6; 1.4)	10	(4.1; 3.1)	33
03/06	(3.8; 2.9)	31	(3.1; 2.1)	16	(4.5; 3.7)	38
04/06	(3.5; 2.6)	29	(2.8; 1.8)	13	(4.3; 3.2)	34

magnitude smaller. Interestingly, the red clouds are less spread along the FAR values than the green clouds. This proves that false detections are pretty homogeneous in space and time. On the contrary, green clouds are more spread. This fact can be partially related to the daily distribution of, for example, uncooperative ship traffic. Finally, the T2T-A/F cloud (blue) spreads along larger ToTs, with intermediate FARs. Anyway, its distribution is closer to the JPDA-UKF of Palmaria than that of San Rossore. For completeness, average values are reported in Table III. The T2T-A/F strategy allows to improve single-sensor performance of about 6% and 21% on average w.r.t. Palmaria and San Rossore, respectively, at a bearable increase of the FAR (i.e., 2.2×10^{-11} s$^{-1} \cdot$ m^{-2} versus 1.3×10^{-11} and 1.2×10^{-11} s$^{-1} \cdot$ m^{-2}, respectively).

E. TF and ToT Analysis

For all the days of recording and for all the ships, the number of radar subtracks composing each ship route is extracted. The related mean and standard deviation are then evaluated over all the ship trajectories. Results are jointly compared with the average daily ToT estimates, as summarized in Table IV.

Reported values show that the JPDA-UKF at Palmaria, probably due to a more favorable ship-sensor geometry, performs better than the JPDA-UKF at San Rossore (see columns 3 and 5). However, this result is paid with just a small increase in TF (see columns 2 and 4). In other words, Palmaria provides

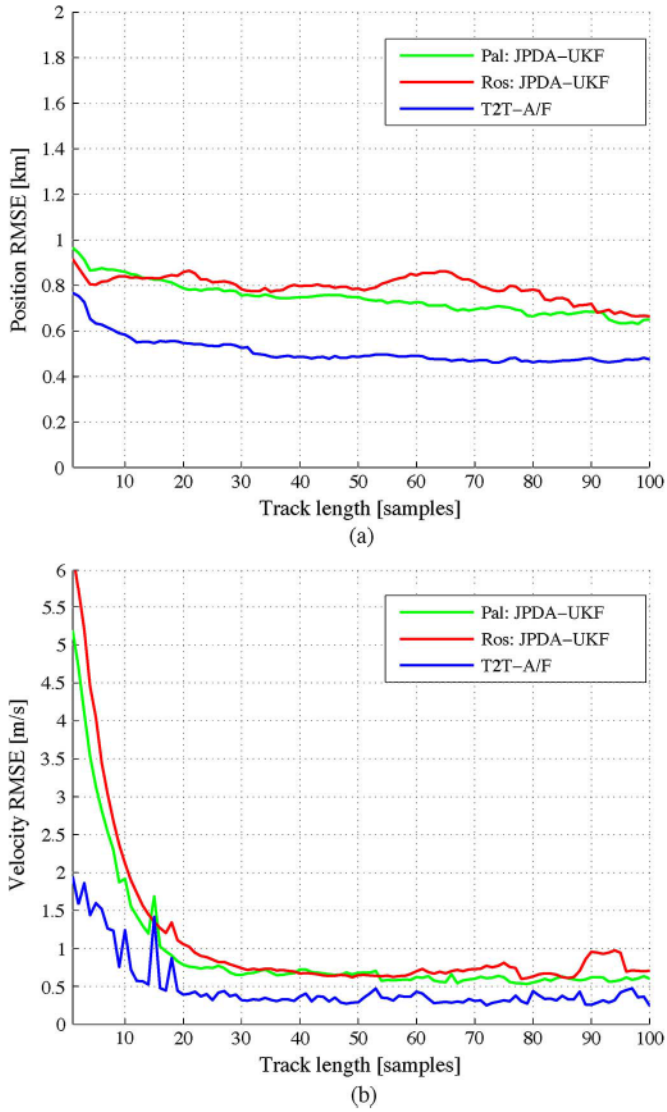

Fig. 10. RMSE of the (a) position and (b) velocity state vector components: (Green) Palmaria JPDA-UKF, (red) San Rossore JPDA-UKF, and (blue) T2T-A/F. (a) RMSE for position. (b) RMSE for velocity.

significantly better ToT than San Rossore, being almost equal the N^{TF}. This is a further proof that the HF-radar installation at Palmaria exhibits a more favorable geometry than the one at San Rossore. Anyway, it is worth noting that a percentage of fragmented tracks come also from the hourly stop and go procedure (lasting about 4 min) that allows the two WERA systems to search for a new HF channel to transmit and receive (see [36]). Finally, the T2T-A/F algorithm improves both trackers in terms of average ToT (see column 7). This improvement is about 5%–10% w.r.t. Palmaria and 15%–25% w.r.t. San Rossore, respectively, as discussed also in Section V-B. Accordingly, also the N^{TF} statistics increase, but this fact is due to the *union* of the two sensors' outputs.

F. Tracking Error Analysis

The RMSE is computed w.r.t. track length for both the position (i.e., x, y) and velocity (i.e., $\dot{x}, \dot{y}$) pair components of the target state vector [see (2)]. Results are shown in Fig. 10,

in subfigures (a) and (b), respectively. Only the event in which the track-to-track fusion effectively happens is considered. The blue curves are obtained averaging the subtracks of the T2T-A/F system. We consider only tracks whose lengths are shorter than 100 samples. The green and red curves are obtained from the *parent tracks* at Palmaria and San Rossore, respectively. The case in which the T2T-A/F strategy relies on just one radar track has demonstrated that the T2T-A/F error closely follows the single-sensor performance. For brevity, these results have been omitted.

Let us consider the RMSE of the position estimate [see Fig. 10(a)]. The error spans between 0.6 and 1.0 km, for both Palmaria (green) and San Rossore (red). As expected, the errors of the two stand-alone systems are pretty close, while the T2T-A/F system (blue) provides an RMSE significantly below that of the two JPDA-UKFs, about 200–300 m on average. Further information about the placement of the AIS transponder (i.e., from-bow and from-port distances) has not been considered. We assumed that the corrections were null on average.

The RMSE of the velocity estimate is presented in Fig. 10(b). Between the DF output and the two trackers, significant differences arise, not only in terms of mean error level (about 0.5 m/s smaller) but also in terms of transitory error, almost eliminated by the T2T fusion algorithm. In fact, when one of the two sensors loses its track, the other one most likely is able to follow it.

In particular, this fact can be well observed in Fig. 11 for a typical commercial ship route. For clarity, the trajectory of the German cargo ship Finlandia (158 m long and 25 m wide), displaying Maritime Mobile Service Identity (MMSI) number 218033000 and crossing the fusion region on May 12, 2009, is depicted in Fig. 12.

Both the errors on the position and velocity estimates are shown in Fig. 11(a) and (b), respectively. When track fusion is effectively carried out (e.g., between 01:20 and 02:00 and between 03:00 and 03:20 UTC), the transitory phases are almost eliminated, as shown in Fig. 11(b). This is in agreement to what is shown in Fig. 10. On average, the T2T-A/F estimate is significantly better, in terms of both ToT and estimate accuracy [see Fig. 11(a) and (b)]. Time intervals in which the T2T-A/F output relies on one sensor only can be observed as well. As to be expected, in these cases, the errors coincide with the single-sensor outputs.

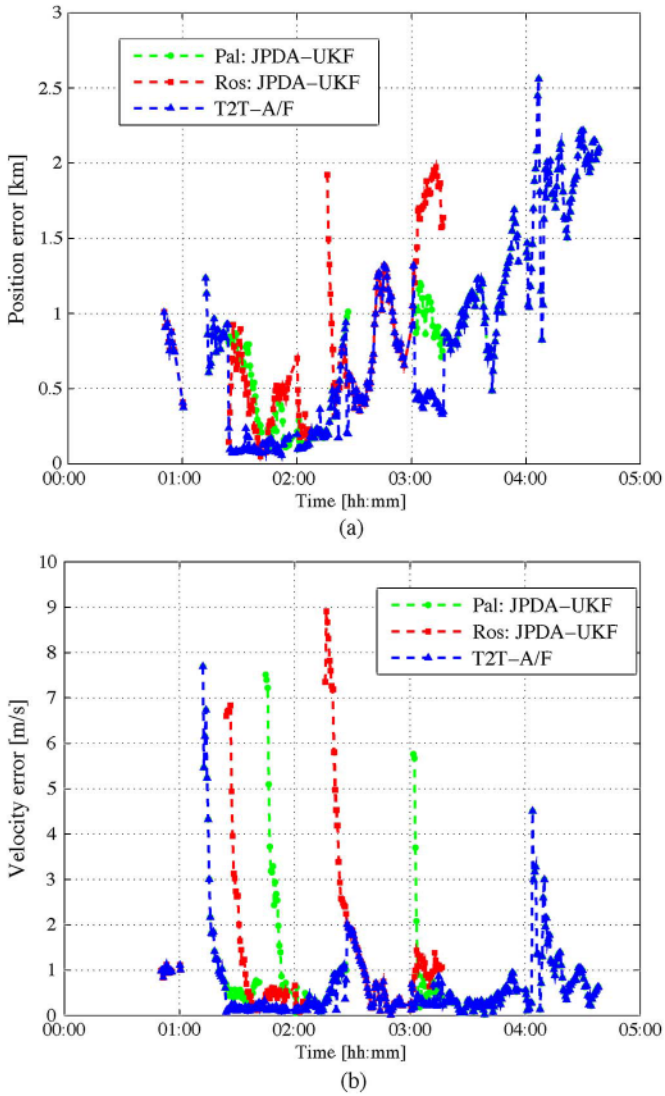

Fig. 11. Ship route, position, and velocity errors for ship with MMSI 218033000 on May 12, 2009: (Green) Palmaria JPDA-UKF, (red) San Rossore JPDA-UKF, and (blue) T2T-A/F.

VI. Conclusion and Outlook

In this paper, a maritime-surveillance system based on two simultaneously operating HFSW radars has been presented, and its performance has been evaluated by means of experimental data. AIS position reports from cooperative vessels have been considered as ground-truth data. A whole processing chain has been considered, going from the OS-CFAR detection algorithm to the JPDA-UKF tracking filter to the T2T-A/F, applied to exploit the aspect diversity of the two radar installations.

To assess system performance, a methodology for validating the outputs (i.e., both detections and tracks) and a set of *ad hoc* performance metrics have been proposed and motivated. These metrics (i.e., ToT, FAR, accuracy, and TF) have been evaluated for both static (e.g., ship length) and kinematic (e.g., range, azimuth, and range rate) information and averaged over about one month of recorded data.

Single-sensor performance has been estimated first, and the JPDA-UKF tracking algorithm has been compared with the OS-CFAR detector. In terms of average ToT, as expected, both the detector and the tracker have achieved similar results. Conversely, the tracking algorithm has reduced the FAR from 8×10^{-11} to 1.3×10^{-11} $\mathrm{s}^{-1} \cdot \mathrm{m}^{-2}$ and from 10×10^{-11} to 1.2×10^{-11} $\mathrm{s}^{-1} \cdot \mathrm{m}^{-2}$ at Palmaria and San Rossore, respectively.

The T2T-A/F strategy has demonstrated its effectiveness w.r.t. the single-sensor JPDA-UKF, in terms of increased ToT (about 6% w.r.t. Palmaria and 21% w.r.t. San Rossore on average) and reduced RMSE (about 200 m and 0.5 m/s for position and velocity estimates). Moreover, aspect diversity has made it possible to overcome the problem of the blind Doppler zones around the first-order Bragg velocities and other geometry-related issues. Concluding, during the experimentation,

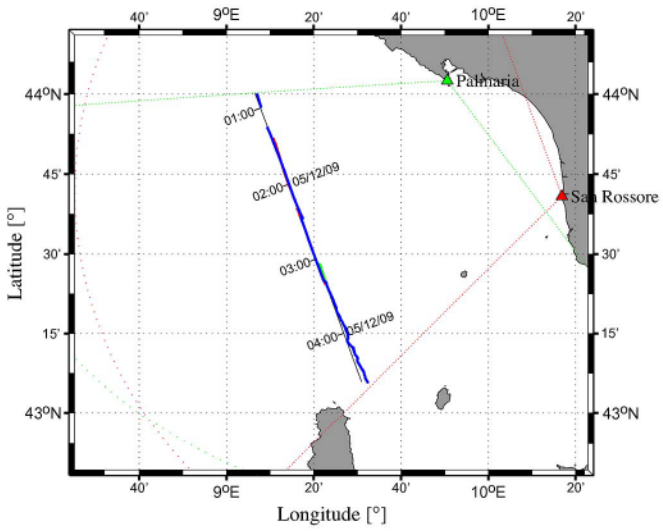

Fig. 12. Typical commercial ship route. Cargo ship Finlandia (MMSI 218033000) crossing the fusion region on May 12, 2009 is depicted: (Black) AIS trajectory, (blue) T2T-A/F, (green) Palmaria, and (red) San Rossore. (a) Position error. (b) Velocity error.

it was possible to track, up to a 150 km distance, ships $100 \div 250$ m long with ToT $= 40\%$ and ships longer than 250 m with ToT $= 55\%$ on average.

On the other hand, these improvements have led to an increase of both TF (i.e., the average of daily subtracks per ship) and FAR. About the former metric, values of 3.94 and 3.65 have been respectively estimated at Palmaria and San Rossore, and a value of about 4.61 has been estimated at the T2T-A/F system. An increase of the FAR has been observed as well, from 1.3×10^{-11} and 1.2×10^{-11} $\mathrm{s}^{-1} \cdot \mathrm{m}^{-2}$ at Palmaria and San Rossore to 2.2×10^{-11} $\mathrm{s}^{-1} \cdot \mathrm{m}^{-2}$ after T2T fusion. Fortunately, the estimated FAR represented an upper bound of the real FAR since many vessels in the surveyed area had no AIS transponder. This analysis has proven that the ship-sensor relative geometry at Palmaria was more favorable than the one at San Rossore.

The aforementioned results have demonstrated that low-power HFSW radar systems, not intended for maritime-surveillance purposes, can take advantage from more advanced signal processing techniques and from aspect diversity for providing additional information on the maritime picture with no additional costs on the system setup.

Anyway, several issues still remain open, and among these are the estimation of the number of vessels not carrying any AIS transponder and the possibility to exploit multiple model-based techniques for tracking maneuvering targets (e.g., fishing and luxury boats). Furthermore, a procedure for correcting the position estimates, based on the from-bow and from-port distances of the AIS transponder, is currently ongoing.

Acknowledgment

The authors would like to thank the anonymous reviewers for valuable suggestions and corrections which allowed to improve the quality of the paper.

References

[1] S. Grosdidier, A. Baussard, and A. Khenchaf, "HFSW radar model: Simulation and measurement," *IEEE Trans. Geosci. Remote Sens.*, vol. 48, no. 9, pp. 3539–3549, Sep. 2010.

[2] S. Rotheram, "Ground-wave propagation. Part 1: Theory for short distances," *Proc. Inst. Elect. Eng. F—Commun. Radar Signal*, vol. 53, no. 5, pp. 275–284, Oct. 1981.

[3] S. Rotheram, "Ground-wave propagation. Part 2: Theory for medium and long distances and reference propagation curves," *Proc. Inst. Elect. Eng. F—Commun. Radar Signal*, vol. 53, no. 5, pp. 285–295, Oct. 1981.

[4] K.-W. Gurgel, A. Dzvonkovskaya, T. Pohlmann, T. Schlick, and E. Gill, "Simulation and detection of tsunami signatures in ocean surface currents measured by HF radar," *Ocean Dyn.*, vol. 61, no. 10, pp. 1495–1507, Oct. 2011.

[5] D. E. Barrick and M. W. Evans, "Implementation of coastal current-mapping HF radar system," U.S. Dept. Commerce, Washington, DC, USA, Tech. Rep. 1, 1976.

[6] K.-W. Gurgel, G. Antonischki, H.-H. Essen, and T. Schlick, "Wellen radar (WERA): A new ground-wave based HF radar for ocean remote sensing," *Coastal Eng.*, vol. 37, no. 3, pp. 219–234, Aug. 1999.

[7] K.-W. Gurgel and T. Schlick, "HF radar wave measurements in the presence of ship echoes—Problems and solutions," in *Proc. Oceans Europe*, Brest, France, Jun. 2005, pp. 937–941.

[8] R. H. Khan, "Ocean-clutter model for high-frequency radar," *IEEE J. Ocean. Eng.*, vol. 16, no. 2, pp. 181–188, Apr. 1991.

[9] R. J. Martin and M. J. Kearney, "Remote sea current sensing using HF radar: An autoregressive approach," *IEEE J. Ocean. Eng.*, vol. 22, no. 1, pp. 151–155, Jan. 1997.

[10] K.-W. Gurgel and G. Antonischki, "Remote sensing of surface currents and waves by the HF radar WERA," in *Proc. 7th IEE Conf. Electron. Eng. Oceanogr.*, Southampton, U.K., Jul. 1997, pp. 211–217.

[11] L. Sevgi, A. Ponsford, and H. Chan, "An integrated maritime surveillance system based on high-frequency surface-wave radars. 1. Theoretical background and numerical simulations," *IEEE Antennas Propag. Mag.*, vol. 43, no. 4, pp. 28–43, Aug. 2001.

[12] A. Ponsford, L. Sevgi, and H. Chan, "An integrated maritime surveillance system based on high-frequency surface-wave radars. 2. Operational status and system performance," *IEEE Antennas Propag. Mag.*, vol. 43, no. 5, pp. 52–63, Oct. 2001.

[13] S. Maresca, M. Greco, F. Gini, R. Grasso, S. Coraluppi, and N. Thomas, "The HF surface wave radar WERA. Part I: Statistical analysis of recorded data," in *Proc. IEEE Radar Conf.*, Washington, DC, USA, 2010, pp. 826–831.

[14] S. Maresca, M. Greco, F. Gini, R. Grasso, S. Coraluppi, and N. Thomas, "The HF surface wave radar WERA. Part II: Spectral analysis of recorded data," in *Proc. IEEE Radar Conf.*, Washington, DC, USA, 2010, pp. 969–974.

[15] Y. Bar-Shalom, P. Willett, and X. Tian, *Tracking and Data Fusion: A Handbook of Algorithms*. Storrs, CT, USA: YBS Publishing, 2011.

[16] R. Mahler, *Statistical Multisource-Multitarget Information Fusion*. Norwood, MA, USA: Artech House, 2007.

[17] S. Blackman and R. Popoli, *Design and Analysis of Modern Tracking Systems*. Norwood, MA, USA: Artech House, 1999.

[18] Y. Bar-Shalom, F. Daum, and J. Huang, "The probabilistic data association filter," *IEEE Control Syst.*, vol. 29, no. 6, pp. 82–100, Dec. 2009.

[19] O. Cappe, S. Godsill, and E. Moulines, "An overview of existing methods and recent advances in sequential Monte Carlo," *Proc. IEEE*, vol. 95, no. 5, pp. 899–924, May 2007.

[20] M. Morelande, C. Kreucher, and K. Kastella, "A Bayesian approach to multiple target detection and tracking," *IEEE Trans. Signal Process.*, vol. 55, no. 5, pp. 1589–1604, May 2007.

[21] B.-T. Vo, B.-N. Vo, and A. Cantoni, "Bayesian filtering with random finite set observations," *IEEE Trans. Signal Process.*, vol. 56, no. 4, pp. 1313–1326, Apr. 2008.

[22] P. Braca, S. Marano, V. Matta, and P. Willett, "Asymptotic efficiency of the PHD in multitarget/multisensor estimation," *IEEE J. Sel. Topics Signal Process.*, vol. 7, no. 3, pp. 553–564, Jun. 2013.

[23] P. Braca, S. Marano, V. Matta, and P. Willett, "Multitarget-multisensor ML and PHD: Some asymptotics," in *Proc. 15th Int. Conf. Inf. FUSION*, Singapore, 2012, pp. 2347–2353.

[24] P. Braca, S. Marano, V. Matta, and P. Willett, "A linear complexity particle approach to the exact multi-sensor PHD," in *Proc. IEEE ICASSP*, Vancouver, Canada, May 2013, pp. 4061–4065.

[25] S. Coraluppi and D. Grimmett, "Multistatic sonar tracking," in *Proc. SPIE Conf. Signal Proc., Sensor Fusion, Target Rec. XII*, Orlando, FL, USA, Apr. 2003, pp. 399–410.

[26] A. Dore, M. Soto, and C. Regazzoni, "Bayesian tracking for video analytics," *IEEE Signal Process. Mag.*, vol. 27, no. 5, pp. 46–55, Sep. 2010.
[27] G. W. Pulford, "Taxonomy of multiple target tracking methods," *Proc. Inst. Elect. Eng.— Radar Sonar Navig.*, vol. 152, no. 5, pp. 291–304, Oct. 2005.
[28] A. Dzvonkovskaya, K.-W. Gurgel, H. Rohling, and T. Schlick, "Low power high frequency surface wave radar application for ship detection and tracking," in *Proc. Int. Conf. Radar*, Adelaide, SA, USA, 2008, pp. 627–632.
[29] S. J. Julier and J. K. Uhlmann, "Unscented filtering and nonlinear estimation," *Proc. IEEE*, vol. 92, no. 3, pp. 401–422, Mar. 2004.
[30] P. Braca, R. Grasso, M. Vespe, S. Maresca, and J. Horstmann, "Application of the JPDA-UKF to HFSW radars for maritime situational awareness," in *Proc. 15th Int. Conf. Inf. FUSION*, Singapore, 2012, pp. 2585–2592.
[31] P. Braca, M. Vespe, S. Maresca, and J. Horstmann, "A novel approach to high frequency radar ship tracking exploiting aspect diversity," in *Proc. IEEE IGARSS*, Munich, Germany, 2012, pp. 6895–6898.
[32] J. Headrick and M. Skolnik, "Over-the-horizon radar in the HF band," *Proc. IEEE*, vol. 62, no. 6, pp. 664–673, Jun. 1974.
[33] X. R. Li and V. Jilkov, "Survey of maneuvering target tracking. Part I. Dynamic models," *IEEE Trans. Aerosp. Electron. Syst.*, vol. 39, no. 4, pp. 1333–1364, Oct. 2003.
[34] L. Bruno, P. Braca, J. Horstmann, and M. Vespe, "Experimental evaluation of the range-Doppler coupling on HF surface wave radars," *IEEE Geosci. Remote Sens. Lett.*, vol. 10, no. 4, pp. 850–854, Jul. 2013.
[35] "Regulation 19," Safety of Life at Sea (SOLAS) Convention.
[36] K.-W. Gurgel, Y. Barbin, and T. Schlick, "Radio frequency interference suppression techniques in FMCW modulated HF radars," in *Proc. Oceans Europe*, Aberdeen, U.K., 2007, pp. 1–4.

Salvatore Maresca was born in La Spezia, Italy, in 1980. He received the M.S. degree in telecommunications engineering and the Ph.D. degree in information engineering from the University of Pisa, Pisa, Italy, in 2006 and 2010, respectively.

In July 2010, he has joined the NATO Science and Technology Organization Centre for Maritime Research and Experimentation, as a Visiting Researcher. His research activity develops in the context of maritime situational awareness, and his main interests are in statistical signal processing, with a focus on detection and estimation theory, target tracking, and data fusion algorithms.

Paolo Braca received the Laurea degree (summa cum laude) in electronic engineering and the Ph.D. degree (highest rank) in information engineering from the University of Salerno, Salerno, Italy, in 2006 and 2010, respectively.

In 2009, he has been a Visiting Scholar at the Electrical and Computer Engineering department of the University of Connecticut, Storrs, CT, USA. In 2010, he joined D'Appolonia S.p.A., Rome, Italy, as a Senior Engineer. In 2010–2011, he has been a Postdoctoral Associate at the University of Salerno. He is currently a Scientist at the Research Department of the NATO Science and Technology Organization Centre for Maritime Research and Experimentation (formerly Supreme Allied Commander Atlantic Research Centre (SACLANTCEN) and NATO Undersea Research Centre (NURC)). His main research interests include statistical signal processing with emphasis on detection and estimation theory, wireless sensor networks, multiagent algorithms, target tracking, and data fusion.

Dr. Braca acts as a reviewer for many international journals and conferences and is a member of the Multistatic Tracking Working Group, International Society of Information Fusion. He has been a Co-organizer with Prof. Peter K. Willett of the special session Multi-Sensor Multi-Target Tracking at the European Signal Processing Conference 2013. He was the recipient of the Best Student Paper Award (second place) at the 12th Conference on Information Fusion in 2009.

Jochen Horstmann received the Diplom (Dipl.-Oz.) degree in physical oceanography and the Ph.D. (Dr.rer.nat.) degree in earth sciences from the University of Hamburg, Hamburg, Germany, in 1997 and 2002, respectively.

He was with GKSS Research Center, Geesthacht, Germany, where he joined the Coupled Model Systems group in 1995 and has been a Research Scientist since 2002. In 2002, he was a Visiting Scientist with the Applied Physics Laboratory of the John Hopkins University, Laurel, MD, USA, and with the National Environmental Satellite, Data, and Information Service of NOAA, Washington, DC, USA. In 2004 and 2005, he was a Visiting Scientist with the Center for Southeastern Tropical Advanced Remote Sensing of the University of Miami, FL, USA. Since 2007, he has been an Adjunct Professor with the Rosenstiel School of Marine and Atmospheric Science, University of Miami, FL, USA. From 2008 to 2013, he was a Senior Remote Sensing Scientist with the Center for Maritime Research and Experimentation of the NATO Science and Technology Organization in La Spezia, Italy. Since 2013, he has been the Head of the Department of Radar Hydrography at the Institute for Coastal Research of the Helmholtz Center Geesthacht, Germany. He has a wide experience in the field of radar remote sensing with respect to ocean wind, waves, and currents and has authored and coauthored more than 150 scientific and technical publications, reports, and book articles, of which 37 have been published in international peer-reviewed journals. His main research interests are the development of oceanographic applications using radar-based sensors to investigate ocean surface and subsurface processes.

Raffaele Grasso received the M.S. degree in telecommunication engineering from the University of Pisa, Pisa, Italy, in 1996 and the Ph.D. degree in remote sensing from the University of Florence, Florence, Italy, in 2000.

He is a Scientist at the Research Department of the NATO Science and Technology Organization Centre for Maritime Research and Experimentation (CMRE, formerly SACLANTCEN and NURC). He was a consultant at CMRE from 2002 to 2006 and a consultant at the University of Pisa from 2000 to 2001. His main research interests include statistical signal processing, information fusion, sensor networks, radar, underwater autonomous vehicles, compressive sensing, and decision support systems for operation planning.

Document Data Sheet

Security Classification		Project No.
Document Serial No.	**Date of Issue**	**Total Pages**
CMRE-PR-2014-014	May 2014	16 pp.

Author(s)

Maresca, S., Braca, P., Horstmann, J., Grasso R.

Title

Maritime surveillance using multiple high-frequency surface-wave radars.

Abstract

In the last decades, great interest has been directed toward low-power high-frequency (HF) surface-wave radars as long-range early warning tools in maritime-situational-awareness applications. These sensors, developed for ocean remote sensing, provide an additional source of information for ship detection and tracking, by virtue of their over-the-horizon coverage capability and continuous-time mode of operation. Unfortunately, they exhibit many shortcomings that need to be taken into account, such as poor range and azimuth resolution, high nonlinearity, and significant presence of clutter. In this paper, radar detection, multitarget tracking, and data fusion (DF) techniques are applied to experimental data collected during an HF-radar experiment, which took place between May and December 2009 on the Ligurian coast of the Mediterranean Sea. The system performance is defined in terms of time on target (ToT), false alarm rate (FAR), track fragmentation, and accuracy. A full statistical characterization is provided using one month of data. The effectiveness of the tracking and DF procedures is shown in comparison to the radar detection algorithm. In particular, the detector's FAR is reduced by one order of magnitude. Improvements, using the DF of the two radars, are also reported in terms of ToT as well as accuracy.

Keywords

Data fusion (DF), high-frequency (HF) surface wave (HFSW) radar, maritime surveillance, sea clutter, target detection, target tracking.

Issuing Organization

Science and Technology Organization
Centre for Maritime Research and Experimentation

Viale San Bartolomeo 400, 19126 La Spezia, Italy

[From N. America:
STO CMRE
Unit 31318, Box 19, APO AE 09613-1318]

Tel: +39 0187 527 361
Fax:+39 0187 527 700

E-mail: library@cmre.nato.int